PNAS
www.pnas.org

Supplementary Information for

Integrative analysis of gene expression, DNA methylation, physiological traits, and genetic variation in human skeletal muscle

D. Leland Taylor[1,2], Anne U. Jackson[3,4], Narisu Narisu[1], Gibran Hemani[5], Michael R. Erdos[1], Peter S. Chines[1], Amy Swift[1], Jackie Idol[1], John P. Didion[1], Ryan P. Welch[3,4], Leena Kinnunen[6], Jouko Saramies[7], Timo A. Lakka[8,9,10], Markku Laakso[11,12], Jaakko Tuomilehto[6,13,14], Stephen C. J. Parker[15,16], Heikki A. Koistinen[6,17,18], George Davey Smith[5], Michael Boehnke[3,4], Laura J. Scott[3,4,*], Ewan Birney[2,*], Francis S. Collins[1,*]

1. Medical Genomics and Metabolic Genetics Branch Branch, National Human Genome Research Institute, National Institutes of Health, Bethesda, MD 20892, USA
2. European Molecular Biology Laboratory, European Bioinformatics Institute, Wellcome Trust Genome Campus, Hinxton, Cambridgeshire CB10 1SD, UK
3. Department of Biostatistics, School of Public Health, University of Michigan, Ann Arbor, MI 48109, USA
4. Center for Statistical Genetics, University of Michigan, Ann Arbor, MI 48109, USA
5. MRC Integrative Epidemiology Unit, Population Health Sciences, University of Bristol, Bristol BS8 2BN, UK
6. Department of Public Health Solutions, National Institute for Health and Welfare, Helsinki FI-00271, Finland
7. Rehabilitation Center, South Karelia Social and Health Care District EKSOTE, Lappeenranta FI-53130, Finland
8. Institute of Biomedicine, School of Medicine, University of Eastern Finland, Kuopio Campus, Kuopio FI-70211, Finland
9. Department of Clinical Physiology and Nuclear Medicine, Kuopio University Hospital, Kuopio FI-70211, Finland
10. Foundation for Research in Health Exercise and Nutrition, Kuopio Research Institute of Exercise Medicine, Kuopio FI-70100, Finland
11. Institute of Clinical Medicine, Internal Medicine, University of Eastern Finland, Kuopio FI-70210, Finland
12. Department of Medicine, Kuopio University Hospital, Kuopio FI-70210, Finland
13. Department of Public Health, University of Helsinki, Helsinki FI-00014, Finland
14. Saudi Diabetes Research Group, King Abdulaziz University, Jeddah 21589, Saudi Arabia
15. Department of Computational Medicine and Bioinformatics, University of Michigan, Ann Arbor, MI 48109, USA
16. Department of Human Genetics, University of Michigan, Ann Arbor, MI 48109, USA
17. Department of Medicine, University of Helsinki and Helsinki University Central Hospital, Helsinki FI-00029, Finland
18. Minerva Foundation Institute for Medical Research, Helsinki FI-00290, Finland

* To whom correspondence should be addressed. Email: ljst@umich.edu, birney@ebi.ac.uk, or collinsf@mail.nih.gov.

This PDF file includes:

- Supplementary Notes
- Supplementary Materials and Methods
- Supplementary Figures S1 to S34
- Supplementary Tables S1 to S7
- Captions for Supplementary Datasets S1 to S5
- References for SI reference citations

Other supplementary materials for this manuscript include the following:

- Supplementary Datasets S1 to S5

Supplementary Notes

Note S1. We note that using genetic colocalization to distinguish model 1 can be unreliable if: 1) the LD patterns between the FUSION study and the GWAS differ, 2) there are multiple conditionally independent causal variants within the same locus, or 3) the LD between two causal variants for the exposure and the outcome is extremely high (r^2 close to 1). Only experimental work can truly pinpoint the causal SNV(s).

Note S2. Biological knowledge of the instrument SNV can be used to guard against the possibility of reverse causation in an MR analysis. For instance, in cases where a molecular trait (e.g., gene expression or DNAme) is modelled as an exposure and a disease/quantitative trait (e.g., BMI) as the outcome, it is reasonable to assume a low probability that a SNV with a strong molecular trait association primarily affects the disease/quantitative trait and subsequently the molecular trait, especially given a polygenic disease/quantitative trait composed of many small genetic effects. The genetic effect on the disease/quantitative trait and molecular trait could be independent (horizontal pleiotropy), but the SNV is unlikely to affect the molecular trait *through* the disease/quantitative trait.

By contrast, when considering two molecular traits and a SNV whose biological effect is not well understood, one cannot assume the criteria of MR are met. Indeed, studies have reported instances where DNAme drives expression (an active model) as well as the reverse (a passive model) (1, 2). Triangulating between different methods in this scenario is important. By comparing the variance explained by the SNV through a statistical test, the MR Steiger test infers the causal direction between molecular traits when the biological effect of the SNV (instrument variable) is not fully understood. However, the MR Steiger test cannot distinguish between a causal and independent model (horizontal pleiotropy). The CIT can distinguish between a causal and independent model (Fig. S19) but is less reliable in the presence of measurement error (which could be technical or biological) compared to MR (3). In particular, measurement error in the mediating variable is likely to bias CIT results towards declaring two molecular traits as causally independent.

Supplementary Materials and Methods

Participant recruitment, muscle biopsy procedures, physiological trait phenotyping are described in Scott et al. (4).

Genotyping and quality control

We extracted DNA from blood. DNA samples were genotyped at the Genetic Resources Core Facility of the Johns Hopkins Institute of Genetic Medicine. 327 samples were genotyped on the HumanOmni2.5-4v1_H BeadChip array and four on the InfiniumOmni2-5Exome-8v1-3 BeadChip array (Illumina, San Diego, CA, USA). We mapped the Illumina array probe sequences to the hg19 genome assembly using the Burrows-Wheeler Aligner (5). We excluded SNVs not present on both arrays, SNVs with probe alignment problems (e.g., multi-mapping probes), and probes with known SNVs in the 3' end. We excluded SNVs with call rates <95%, minor allele count (MAC) <1, or Hardy–Weinberg equilibrium (HWE) p-value<10^{-4}, leaving 1,571,557 SNVs. Alleles were oriented relative to the reference genome.

We assessed sample relatedness using KING (6) and identified two pairs (normal glucose tolerant-impaired glucose tolerance) of first-degree relatives. For each pair, we excluded the normal glucose tolerant participant. To assess Finnish ancestry, we estimated genetic principal components (PCs) using weights produced using the Population Reference Sample (POPRES) European reference panel (7) in LASER (8). We compared PCs from our samples to those of the reference populations. We removed one non-Finnish participant (Table S5). To control for population stratification in the QTL analyses, we performed principal component analysis (PCA) (9) using 437,182 genotyped, autosomal SNVs that remained after pruning SNVs to a pairwise r^2 threshold of 0.5, excluding SNVs with minor allele frequency (MAF) ≤1%, and regions of high LD (10, 11).

Genotype imputation

Prior to genotype imputation we removed a) SNVs with a difference in alternate allele frequency between FUSION and phase 3 1000G European samples >20%, b) palindromic SNVs with MAF >40%, or c) SNVs with genotype missingness >2.5%, leaving 1,543,123 SNVs. We performed pre-phasing and imputation on autosomal SNVs using the Michigan Imputation Server (12). We used Eagle v2.3 (13) for SNV pre-phasing. We imputed SNV genotype dosages using minimac3 (12) and the Haplotype Reference Consortium (hrc.r1.1.2016, build GRCh37/hg19) panel (14). We included 7,128,878 autosomal, biallelic SNVs with imputation quality r^2 hat >0.3 and MAC ≥10 in the 318 samples used for QTL analysis (see ***Proximal eQTL and mQTL analysis*** below).

RNA isolation and sequencing

The RNA sequencing design of this study is described in Scott et al. (4). Briefly, we visually dissected 30-50 mg of each frozen muscle biopsy sample (n=323 including seven replicates), avoiding adipose tissue. Total RNA was extracted and purified with Trizol (Invitrogen, Carlsbad, CA). RNA integrity numbers (RINs), an estimate of RNA degradation (15), ranged from 6.6 to 9.4 (median 8.4). We mean imputed the RIN value of one sample missing a RIN value due to a technical error (mean value 8.37). After poly(A) selection, each sample was sequenced to >80 million 100bp paired-end reads. We assessed the uniformity of read depth coverage by calculating the mean transcript integrity number (TIN) (16) for each sample using RSeQC v2.6.4 (17).

RNA-seq processing and quality control

We followed the same read mapping and quality control (QC) procedures as in our previous muscle RNA-seq data freeze (4). Using the basic GENCODE v19 annotations (18), we counted fragments mapping to each gene using htseq-count v0.5.4 (19) and quantified gene expression as transcripts per million (TPM) (20, 21).

We performed QC on 323 samples: 279 samples + 7 replicates from Scott et al. (4) and 30 additional samples with sequencing completed after that paper. As in Scott et al. (4), we ran QoRTs v1.1.18 (22). We excluded three samples, in addition to the one excluded by Scott et al. (4), that were extreme outliers based on their read coverage at the 3' end of gene bodies. We reinstated one sample previously excluded in Scott et al. (4) that was no longer an outlier based on insert size in context of the full dataset.

We analyzed the cumulative gene diversity—the cumulative fraction of reads as a function of genes sorted by read-count—across samples. For each gene, we calculated the median counts across samples and used the cumulative distribution of median read counts as the reference distribution. We compared the cumulative read count distribution of each sample to this reference using the Kolmogorov-Smirnov test (ks.test function in R) and removed seven additional outlier samples (p-value<0.01).

To identify sample swaps and contaminated samples we compared the allelic RNA-seq read count distribution to known sample genotypes using verifyBamID v1.1.1 (23). We identified the two pairs of sample swaps and one contaminated sample previously described in Scott et al. (4). We verified the reported sex of the remaining samples using *XIST* gene expression and the mean Y chromosome gene expression.

As a final QC step, we sought to remove outlier samples based on PCA. For each gene, we performed linear regression of gene expression (TPM) as a function of age, sex, batch, and RIN. We performed PCA on the gene expression residuals. We selected the minimum number of PCs to explain 20% of the variance in gene

expression (2 PCs) and transformed the PCs to z-scores. We found no sample outliers, defined as |z-score| >5, for either PC.

After removing the genotype-based sample exclusions, the gene expression analysis set comprised 301 unique samples (Table S6) and 20,953 autosomal genes with ≥5 counts in >25% of samples. For each subsequent analysis with a different sample set (e.g., dichotomous physiological trait association, continuous physiological trait association, eQTM, eQTL), we performed inverse normalization of the TPMs (randomly breaking ties) for each gene (inverse normalized gene expression) for the samples used in that analysis.

DNA isolation and methylation quantification

We measured DNA methylation (DNAme) in 303 skeletal muscle samples with a remaining piece of tissue after performing RNA-seq. Both gene expression and DNAme data come from separate pieces of tissue from the same biopsy site. We visually dissected ~25 mg of each frozen muscle sample, avoiding adipose tissue. We extracted 200 ng of genomic DNA per sample using the DNeasy Blood & Tissue Kits (QIAGEN) according to the manufacturer's recommendations. We bisulfite-converted genomic DNA using EZ DNA methylation Kits (ZYMO research), as part of the TruSeq DNA Methylation protocol (Illumina). We measured DNAme using the Illumina Infinium HD Methylation Assay with Infinium MethylationEPIC BeadChips, according to manufacturer's instructions, at the Center for Inherited Disease Research (Johns Hopkins University). Muscle samples were processed within a larger study including 333 adipose, EndoC-βH1 (pancreatic beta cell line), 41 islets, and 24 whole blood samples.

Methylation blacklist probes identification and exclusion

Prior to sample QC we identified a set of MethylationEPIC BeadChip probes with sequences that may cause problems in subsequent analyses, commonly termed blacklist probes.

Illumina probes can map to more than one genomic location (24–27). To identify cross-reactive, non-uniquely mapping probes, we mapped probes (excluding control and genotype probes) to the bisulfite-converted genome (GRCh37/hg19) using Novoalign ('-b4 -R120' options). We excluded 49,495 probes that did not map to a unique location.

Illumina DNAme probe sequences may contain SNVs which lead to biases in inter-individual studies (24, 25). We identified variants to use for probe exclusions (rules below) from the union of the following sources: 1) common (MAF≥1%) SNVs, indels, or structural variation in the phase 3 1000G European dataset, 2) common SNVs in the HRC reference panel r1.1, and 3) imputed SNVs with a cumulative total of >1 allele in our own samples. We excluded type I and II probes with a variant within 10 bp of the 3' end of the probe (25) or within the target CpG itself. We also excluded type I probes with a variant within the single base extension site. In all we removed 63,840 probes that overlapped an SNV. In addition, we removed all probes

on a previously published blacklist from McCartney et al. (26). In total, we removed 120,627 blacklist probes.

Initial methylation sample quality control

We processed raw signal idat files using minfi v1.20.2 (28) and calculated beta-values and M-values using the Illumina normalization method implemented in minifi (default parameters). We excluded five samples for which >1% of probes had low quality signal, defined as a probe detection p-value >0.05—which compares the combined raw methylated (Meth) and un-methylated (Unmeth) signal to the background noise (28, 29). For each sample, we calculated the median signal intensity of the Meth and Unmeth signals (28); we removed any sample with Meth and/or Unmeth <10 (n=1). We analyzed signals from sets of control probes designed to capture different technical aspects (e.g., hybridization efficiency, staining) using the returnControlStat function from shinyMethyl v1.10.0 (30). For each control probe type, we calculated the mean signal of each sample. To identify samples with evidence of multiple outlying probe signals we transformed the mean sample signal for each control probe type to z-scores and removed three muscle samples with |z-score| >3 for ≥1 type of control probes.

We assessed the 59 probes designed to detect common SNVs on the EPIC array (SNV probes) to verify sample identity. From these 59 SNV probes, we dropped: 1) two probes with an SNV from the Haplotype Reference Consortium within the last 10bp of the probe, 2) six that failed HWE (p-value<10^{-6}), 3) one with many beta-values in-between genotype clusters, 4) one that was tri-allelic in the HRC reference panel, and 5) two with >10 mismatches across samples. In total, we compared 47 SNVs to imputed genotypes. For each of the 47 SNV probes, we converted the beta-values for the proportion of a given allele (0, 0.5, 1) to the 0, 1, 2 scale of genotype dosages oriented to the alternate allele. For each sample, we calculated the total allelic difference of the EPIC array genotype dosages and the imputation dosages as the sum of the absolute difference ($|genotype_{EPIC} - genotype_{dosage}|$) over all 47 SNV probes. We dropped four muscle samples with total allelic difference >3 and corrected one sample swap.

We verified the reported sex of the remaining samples using X chromosome DNAme (getSex function in minfi).

Final methylation probe and sample quality control

We removed 733 probes with a probe detection p-value >0.05 in ≥5% of muscle samples that passed initial QC filters, leaving 727,141 autosomal probes.

We identified samples with outlying M-value DNAme distributions by a) calculating per sample M-value percentiles separately for type I and II probes and b) comparing each sample to the median M-value distribution using the Kolmogorov–Smirnov test (ks.test function in R). We identified and removed one muscle sample with p-value <0.01.

We performed PCA of the M-values across the complete dataset (including muscle, adipose, EndoC-βH1, islet, and whole blood samples). The first two PCs visually separated the tissue types. We removed three putative muscle samples that did not cluster with the other muscle samples.

We removed additional outliers based on PCA within muscle samples only. First, we performed linear regression of M-values as a function of plate, sentrix position, plate position, age, and sex. Second, we performed PCA on the residual M-values. We selected the minimum number of PCs to explain 20% of the variance (6 PCs) and transformed the PCs to z-scores. We excluded one sample with a |z-score| >5 for PC2. We repeated PCA and found no further outliers.

After removing the genotype-based exclusions, the total DNAme analysis set comprised 282 unique samples (Table S7) and 727,141 autosomal probes. For each subsequent analysis with a different sample set (e.g., dichotomous physiological trait association, continuous physiological trait association, eQTM, mQTL), we performed inverse normalization of the M-values (randomly breaking ties) for each probe (inverse normalized DNAme) for the samples used in that analysis.

Tissue type proportion estimates

We estimated tissue type proportions in the FUSION muscle samples using five GTEx tissues (phs000424.v7.p2) as a reference: “skin not sun exposed suprapubic”, “whole blood”, “adipose subcutaneous”, “muscle skeletal”, and “EBV transformed lymphocytes” (as a proxy for inflammatory processes). We refer to these tissue/cell types as “tissues”. For each gene present in the FUSION muscle samples, we computed the mean TPM per GTEx tissue and estimated tissue type proportions in FUSION muscle samples using the unmix function from DESeq2 v1.18.1 (31). We estimated 0% skin across all samples and subsequently excluded this tissue estimate. We calculated the Pearson correlation coefficient between tissue estimates and inverse normalized expression PCs (see ***RNA-seq processing and quality control***). We used the estimated tissue type proportions (obtained from expression data) for analysis of both gene expression and of DNAme. The DNAme data were obtained from a separate piece of tissue from the same biopsy. As shown in the ***Results*** section and Fig. S2B, the estimated tissue proportions from RNA-seq of a second pieces of tissue for six samples are highly correlated (r>0.88) and thus should provide good estimates for the DNAme data analysis.

Muscle fiber type proportion estimates

In humans, MYH1 (Type 2X) and MYH2 (Type 2A) are the major fast twitch muscle components, and MYH7 (Type 1) is the primary slow twitch muscle component (32). We assume that the TPM count of each gene is proportional to the amount of each fiber type. To estimate muscle fiber type proportions, we divided the expression (TPMs) of each of these genes by the sum of the expression of the three genes. We calculated the Pearson correlation coefficient between fiber estimates and inverse normalized expression PCs (see ***RNA-seq processing and quality***

control). In addition, as shown in the ***Results*** section and Fig. S3B, the estimated fiber type proportions from RNA-seq of a second pieces of tissue for six samples are highly correlated (r>0.98) and thus should provide good estimates for the DNAme data analysis. To further verify that our estimates reflect fiber type differences in muscle, we used expression of Ca^{2+} ATPase A2 and Ca^{2+} ATPase A1, which are markers for oxidative (slow twitch) or glycolytic (fast twitch) fiber, respectively. Ca^{2+} ATPase A2 showed strong correlation with our type 1 (slow twitch) estimate (r=0.71) and Ca^{2+} ATPase A1 with our type 2X (fast twitch) estimate (r=0.59), confirming our estimates reflect fiber type differences in muscle.

Molecular trait association with muscle fiber and tissue types

We tested for association of inverse normalized gene expression (n=301) and DNAme (n=265; of 282 DNAme samples, 265 had RNA-seq data and therefore estimated tissue and fiber type proportions) with estimated tissue and/or fiber type proportions using linear regression. We used an F-test to calculate p-values (lm and anova functions in R).

We describe analysis for gene expression and use the same analysis strategy for DNAme. For individual *i* and gene *j*, let E_{ij} denote the inverse normalized gene expression and $Z_i = \{Z_1, Z_2, ..., Z_c\}^T$ be the vector of c covariates. We tested for association using the linear model:

$$E_{ij} = \alpha_j + F_{i2A}\delta_{2Aj} + F_{i2X}\delta_{2Xj} + Z_i\gamma_j^T + \varepsilon_{ij} \quad (1)$$

where α_j is the intercept, F_{i2A} and F_{i2X} are the 2A and 2X estimated fiber type proportions, δ_{2Aj} and δ_{2Xj} the corresponding regression coefficients, γ_j is the vector of the regression coefficients for the covariates, and ε_{ij} a normally distributed error term with mean 0 and variance $\sigma^2 = 1$. We included as covariates sex, age, smoking status, collection site, RNA sequencing batch, RIN, and mean TIN. We corrected for the number of tests using the Benjamini-Hochberg procedure (33).

We replaced the estimated fiber type proportion with estimated tissue type proportion and repeated the analysis. We replaced the inverse normalized gene expression with inverse normalized DNAme and repeated these analyses using as covariates sex, age, smoking status, collection site, plate, position of slide on plate, and position of array on slide.

Physiological trait association with tissue and fiber type

We tested for association in 301 participants between eight physiological traits (fasting serum insulin, fasting plasma glucose, BMI, WHR, waist, weight, height, and T2D status) with estimated tissue type or muscle fiber type proportions using linear regression for quantitative traits and logistic regression for T2D. We used an F-test to calculate p-values (lm and anova functions in R). We inverse normalized (randomly breaking ties) the quantitative physiological traits denoted as Y_{ip} for

physiological trait *p*. We tested for association of Y_{ip} with estimated fiber type proportion using the linear regression model:

$$Y_{ip} = \alpha_p + F_{i2A}\delta_{2Ap} + F_{i2X}\delta_{2Xp} + Z_i\gamma_p^T + \varepsilon_{ip} \quad (2)$$

where terms are as defined in equation (1) with covariates: sex, age, smoking status, and collection site.

We tested for association of T2D status with estimated fiber type proportion using logistic regression:

$$T_i = \alpha + F_{i2A}\delta_{2A} + F_{i2X}\delta_{2X} + Z_i\gamma^T \quad (3)$$

where terms and covariates are as defined in equation (2).

We repeated these analyses replacing estimated fiber type proportions with estimated tissue type proportions as well as both tissue and fiber type proportions.

Molecular trait association with physiological traits

We tested for association of inverse normalized continuous physiological traits or T2D status with inverse normalized gene expression (n=301) or DNAme (n=265). We describe analysis for gene expression and use the same analysis strategy for DNAme. We tested for association using the linear regression model:

$$Y_{ip} = \alpha_p + E_{ij}\zeta_{jp} + Z_i\gamma_p^T + \varepsilon_{ip} \quad (4)$$

where ζ_{jp} is the regression coefficient for E_{ij} and other terms are defined in equation (1). We included three different sets of variables as covariates: 1) a “base” set: sex, age, smoking status, sample collection site, and batch variables (defined below), 2) a “base” + estimated tissue/cell proportions (“tissue”), and 3) a “base” + “tissue” + estimated muscle fiber type proportions (“fiber”). For gene expression, batch variables correspond to sequencing batch, RIN, and mean TIN. We tested for association of T2D with inverse normalized expression using logistic regression:

$$T_i = \alpha + E_{ij}\zeta_j + Z_i\gamma^T \quad (5)$$

For each physiological trait, we corrected for the number of molecular traits tested using the Benjamini-Hochberg procedure.

We repeated the analysis replacing inverse normalized gene expression with inverse normalized DNAme including as batch variables: plate, position of slide on plate, and position of array on slide.

GO term enrichment analysis

We performed GO enrichment analysis as described previously (4). Briefly, we used RNA-Enrich (34) and the following logistic regression model:

$$logit(\pi_j) = \alpha + P_j\beta + L_j\gamma \qquad (6)$$

where π_j is the probability of GO term membership for gene j, α is the intercept, β is the regression coefficient for association of GO term membership, P_j is the signed -$\log_{10}$(p-value) of the association between the physiological trait and gene expression with inclusion of tissue type (equation 1) or with inclusion of tissue and fiber type as covariates, and γ is the regression coefficient for the GO term membership with L_j, the $\log_{10}$(gene j length). We include L_j in the model to account for the potential confounding effect of gene length on the enrichment test, as longer genes tend to have higher power for expression-trait association and many GO terms contain sets of genes that are substantially longer or shorter than average.

Adjustment for tissue and fiber type typically resulted in stronger GO term category enrichment (Fig. S5-12). However, for WHR, we saw much weaker enrichment of genes related to cellular respiration after adjustment for tissue and fiber type (cellular respiration genes are enriched in type 1 fibers and the estimated proportion of type 1 fibers is lower in people with higher WHR), suggesting that tissue/fiber composition differences by trait levels can explain some of observed gene set enrichment.

eQTM association

We tested for association between inverse normalized gene expression and inverse normalized DNAme using linear regression in 265 samples with LIMIX v1.0.17 (35). We consider the linear model:

$$E_{ij} = \alpha_j + M_{in}\eta_{nj} + Z_i\gamma_j^T + \varepsilon_{ij} \qquad (7)$$

where M_{in} is the inverse normalized DNAme for probe n, η_{nj} the corresponding regression coefficient, and other terms are defined as in equation (1). We controlled for the number of tests using the Benjamini-Hochberg procedure. Because previous eQTM studies use a wide range of window sizes from 50kb to 1Mb (1, 36–38), we initially performed analysis of DNAme sites ≤10Mb of the gene TSS to evaluate the effect of covariate inclusion on shorter (≤1Mb from TSS to probe site) and longer range (>1Mb & ≤10Mb) associations.

We evaluated models with the following sets of covariates: no covariates, known covariates, and PEER factor covariates. For known covariates we used the three covariate sets described in the ***Molecular trait association with physiological traits*** section with batch covariates for gene expression and DNAme.

For the PEER factor-based covariates, we used subsets of the 50 and 30 PEER factors used in eQTL and mQTL analysis respectively (see ***Proximal eQTL and mQTL analysis*** below). In each PEER factor-based analysis, we included equal numbers (x) of gene expression and DNAme PEER factors and label the analysis as "x PEER factors" (e.g., 2 PEER factors means we included 2 gene expression PEER factors and 2 DNAme PEER factors in the analysis). We performed analysis using x PEER factors (where x = {1-10, 15, 20, 25 or 30}). In our final analysis, we used 5 expression/DNAme PEER factors as covariates since the 1-10Mb eQTM discovery rate changed little when correcting for >5 expression/DNAme PEER factors (Fig. S13-14) and to reduce the potential of inducing collider bias, where adjustment for a variable that is correlated with two otherwise uncorrelated variables induces a correlation (39). We also selected a 1Mb window from the TSS, as the eQTM discovery rate was minimal >1Mb (Fig. S13-14) and to be consistent with our QTL mapping window size.

Proximal eQTL and mQTL analysis

We performed QTL analysis using SNVs within 1Mb of the gene body for gene expression or probe locus for DNAme using QTLtools v1.1 (40). A total of 318 samples had gene expression (n=301) and/or DNAme (n=282) data. We included in our analysis 7,128,878 autosomal SNVs that passed QC and had MAC>10 in the 318 samples. We describe the QTL analysis for gene expression; we used the same analysis strategy for DNAme.

To account for unknown biological and technical factors that may add noise to the measured gene expression, we performed factor analysis of the inverse normalized gene expression via PEER v1.0 (41). We used the linear regression model with an additive genetic effect for gene expression:

$$E_{ij} = \alpha_j + G_{is}\beta_{sj} + Z_i\gamma_j^T + \varepsilon_{ij} \qquad (8)$$

where G_{is} is the imputed allele count for SNV *s* for individuals *i*, β_{sj} is the regression coefficient of the imputed allele count for SNV *s,* and other terms are as in equation (1). We included as covariates the first 4 genotype PCs (Eigenstrat p-value <0.1) and increments from 0-100 PEER factors.

We calculated p-values of the regression coefficients accounting for the all tests for a given gene using a beta distribution fit with 100 permutations (for exploratory PEER factor analysis) and 10,000 permutations (for the final analysis), as described in Delaneau et al. (40). We used Storey-Tibshirani FDR (42) to account for the number of genes tested with a threshold of FDR≤1%.

We present eQTL results based on 50 PEER factors as including these factors as covariates maximized the number of genes with an eQTL (FDR≤1%; Fig. S17).

We repeated the analysis replacing inverse normalized gene expression with inverse normalized DNAme (n=282). We present results based on including 30 PEER factors as including these covariates maximized the number of DNAme sites with an mQTL (FDR≤1%; Fig. S17).

Molecular trait Mendelian randomization and causal inference test

Using MR and mediation techniques, we sought to identify DNAme sites whose methylation level may causally influence gene expression (M→E) or vice versa (E→M; analysis diagram in Fig. S18). Starting with 37,464 eQTM gene-DNAme site pairs (FDR≤1%), we retained 31,578 pairs in which at least one molecular trait (gene expression or DNAme) had a QTL (FDR≤1%).

For a single instrument MR test, we defined instrument variable as the top QTL SNV for the molecular trait used as the exposure; thus, when the top eQTL and mQTL SNVs are different, the instrument will be different for the MR test, depending on which molecular trait is used as the exposure. We therefore analyzed each gene-DNAme pair twice, defining the exposure as either gene expression—using the top eQTL SNV (eSNV) as an instrument ($eSNV_{instrument}$)—or DNAme—using the top mQTL SNV (mSNV) as an instrument ($mSNV_{instrument}$).

We performed MR and tested for colocalization using the Summary data-based Mendelian Randomization (SMR; v0.706) software (43) in molecular trait association mode (44) with the FUSION muscle eQTL and mQTL summary statistics. We used 2,737 Europeans (which includes 979 Finns) from the Genetics of Type 2 Diabetes (GoT2D) project (45) to estimate LD. We controlled for the number of tests performed within each exposure model using the Benjamini-Hochberg procedure. We retained 16,122 gene-DNAme site pairs for which $eSNV_{instrument}$ and/or $mSNV_{instrument}$ had both an MR association (FDR≤1%) and evidence of colocalization of gene expression and DNAme genetic signals (i.e., there was not evidence of instrument heterogeneity; $p_{HEIDI}>0.05$).

We used two tests to identify potentially causal relationships where DNAme drives changes in gene expression (M→E) or vice versa (E→M) for each of the 16,122 gene-DNAme site pairs.

First, we used the MR Steiger test (TwoSampleMR R package v0.4.7) (3), which tests for a difference between variance explained by the SNV on the outcome and the exposure using QTL summary statistics. We retained 7,952 gene-DNAme pairs for which $eSNV_{instrument}$ and/or $mSNV_{instrument}$ had a predicted causal direction from the MR Steiger test (FDR≤1%).

Next, we used the CIT v2.2 (46, 47), which performs a series of conditional regression tests. We compared the CIT p-values of a causal model (exposure drives outcome; $p_{CausalCIT}$) to a reverse causal model (outcome drives exposure; $p_{RevCausalCIT}$) using covariates from the eQTM analysis. We ran the CIT twice for each gene-DNAme site-top QTL SNV trio: a) with the defined exposure molecular trait as the exposure ($p_{CausalCIT}$) and b) with the non-exposure molecular trait defined as the

exposure ($p_{RevCausalCIT}$). When gene expression is the exposure ($eSNV_{instrument}$), our CIT models correspond to: a) $eSNV_{instrument}$→gene expression→DNAme ($p_{CausalCIT}$) and b) $eSNV_{instrument}$→DNAme→gene expression ($p_{RevCausalCIT}$). In the case where DNAme is the exposure ($mSNV_{instrument}$), our CIT models correspond to: a) $mSNV_{instrument}$→DNAme→gene expression ($p_{CausalCIT}$) and b) $mSNV_{instrument}$→gene expression→DNAme ($p_{RevCausalCIT}$). We followed procedures from Ng et al. (2) and applied Bonferroni correction to control for the number of tests, *m*, within each $SNV_{instrument}$ model. We predicted the causal direction for 214 gene-DNAme site pairs where ($p_{CausalCIT} \leq 0.01/m$ and $p_{RevCausalCIT} > 0.01/m$) or ($p_{CausalCIT} > 0.01/m$ and $p_{RevCausalCIT} \leq 0.01/m$), removing pairs identified as independent ($p_{CausalCIT} > 0.01/m$ and $p_{RevCausalCIT} > 0.01/m$) or unclassified ($p_{CausalCIT} \leq 0.01/m$ and $p_{RevCausalCIT} \leq 0.01/m$). We note that gene-DNAme site pairs without a putative causal CIT prediction could be truly independent or could have a causal relationship obscured by measurement error (3).

We retained 213 gene-DNAme site pairs with a concordant predicted causal direction between the MR Steiger test and the CIT for a given $SNV_{instrument}$ model. 87 of these 213 gene-DNAme site pairs had a predicted causal direction using both the $eSNV_{instrument}$ and $mSNV_{instrument}$ models, all of which had a concordant predicted causal direction between both $SNV_{instrument}$ models. Our final dataset consisted of 213 putative causal predictions. To reduce redundant gene-DNAme site pairs, we report the exposure model with the minimum QTL p-value.

To test for differences between E→M and M→E gene-DNAme site pairs, we randomly selected a single gene-DNAme site pair for every gene or DNAme site occurring more than once in the data. We used a Wilcoxon rank sum test to test for a difference in the absolute distance between the DNAme site and gene TSS in putatively causal E→M and M→E gene-DNAme site pairs. We annotated the skeletal muscle chromatin state of the DNAme site for each putatively causal gene-DNAme site pair. For each chromatin state, we tested for a difference in the proportion of E→M and M→E gene-DNAme site pairs using Fisher's exact test and controlled for the number of tests using Bonferroni correction.

Gene expression and DNAme-disease/quantitative trait Mendelian randomization test

We sought to identify genes and/or DNAme sites that may causally influence disease/quantitative traits. As sources of genetic regulators for disease/quantitative traits, we used publicly available summary statistics from GWAS meta-analyses for T2D and 11 T2D-related traits, as well as GWAS results for 522 disease/quantitative traits from the UK Biobank (Table S3). For the UK Biobank summary statistics, we selected 522 diseases/quantitative traits from 2,418 total traits (48). Of the 2,418 traits, we excluded: a) 48 traits unlikely to have a genetic basis (Table S4) and b) 1,848 binary traits with <1,250 participants in either the case and control group to avoid spurious results with variants of MAF <1% (49) given the lowest MAF variant from our QTL study is 1.57%.

We performed MR using SMR for each gene and a 1Mb proximal window across all 534 disease/quantitative traits using FUSION eQTLs, FUSION mQTLs, and GTEx eQTLs spanning 48 tissues (v7; http://cnsgenomics.com/software/smr/#DataResource). For each study, tissue, and molecular trait, we used the top eQTL or mQTL SNV as the instrument variable. We used 2,737 Europeans from the GoT2D project to estimate LD. The MR test assumes the instrument is associated with the exposure (50), and therefore is not valid for SNVs weakly (or not at all) associated with a molecular trait. However, to provide a complete reference dataset to publicly share, we ran SMR for all genes and DNAme sites for each tissue, study, and molecular trait regardless of the top QTL p-value (i.e., the QTL may not be strongly associated with the molecular trait; SMR parameters: '--peqtl-smr 1'). For each study, tissue, and molecular trait, we controlled the false positive rate for the number of valid MR tests (lead QTL p-value$\leq 5x10^{-8}$, the SMR default) across all disease/quantitative traits using the Benjamini-Hochberg procedure. We performed the HEIDI test and retained variants without evidence of instrument heterogeneity ($p_{HEIDI}>0.05$). Finally, to directly compare FUSION and GTEx eQTL results, we ran SMR analysis for gene expression each GTEx tissue using the top FUSION muscle eQTL SNV for each gene and calculated FDR per tissue as above.

***RXRA* power analysis**

We estimated the power to detect an *RXRA* MR association for predicted trunk mass in each GTEx tissue in two steps. First, for each GTEx tissue, we simulated 1,000 replicates of an *RXRA*-eQTL using the observed rs6583658 *RXRA*-eQTL effect size in GTEx skeletal muscle ($beta_{GTEX\ muscle}$) and the estimated GTEx tissue standard error of the effect size ($se_{GTEx\ tissue}$). For a given GTEx tissue, we estimated the rs6583658 $se_{GTEx\ tissue}$ as $se_{GTEX\ muscle}$ x $sqrt(n_{GTEX\ muscle}/n_{GTEX\ tissue})$, assuming the allele frequency of rs6583658 had little variability across tissues. We approximated the two-sided eQTL p-value from the $beta_{GTEX\ muscle}/se_{GTEx\ tissue}$ using a t distribution with degrees of freedom = $n_{GTEx\ muscle}$-2. We performed MR for each tissue eQTL with $p\leq 5x10^{-8}$ (as in ***Gene expression and DNAme-disease/quantitative trait Mendelian randomization test***). For each GTEx tissue, we estimated power as number of tests with an MR association (FDR≤1% GTEx tissue cut point estimated in ***Gene expression and DNAme-disease/quantitative trait Mendelian randomization test***) divided by 1,000. For FUSION skeletal muscle we estimated the power detect an *RXRA* MR association for predicted trunk mass as described above using the eQTL effect size and standard error observed in FUSION skeletal muscle.

Gene expression tissue specificity index

We previously developed an expression specificity index (ESI) to measure the cell/tissue type specificity of gene expression (4, 51). Genes with a high ESI are highly and specifically expressed in a single cell/tissue type based on the reference

panel used to generate the index. We previously used this method to identify genes with muscle specific expression patterns based on a muscle expression specificity index (mESI) we generated using 16 tissues from Illumina Human Body Map 2.0 (4).

To calculate mESI values over a more comprehensive reference panel, we applied this method to 48 tissues from GTEx, removing tissues with <25 samples (bladder, ectocervix, endocervix, and fallopian tube). For each gene in each tissue type, we calculated the average expression across samples to build a reference transcriptome panel. With this reference transcriptome panel, we calculated muscle specificity as previously described (4, 51).

Chromatin states and ATAC-seq data

We used publicly available chromatin states (51) and ATAC-seq data (4, 52, 53).

Data availability

We deposited individual-level genotype, RNA-seq, and DNAme data from this study into the database of Genotypes and Phenotypes (dbGaP) with the accession number phs001048.v2.p1; data are available via the repository's standard data access request procedures. EPIC methylation array blacklist probes and summary statistics of physiological trait associations, eQTMs, eQTLs, mQTLs, and disease/quantitative trait MR associations are publicly available at https://fusion.sph.umich.edu/public/tissue_biopsy/share/2018_muscle.

Supplementary Figures

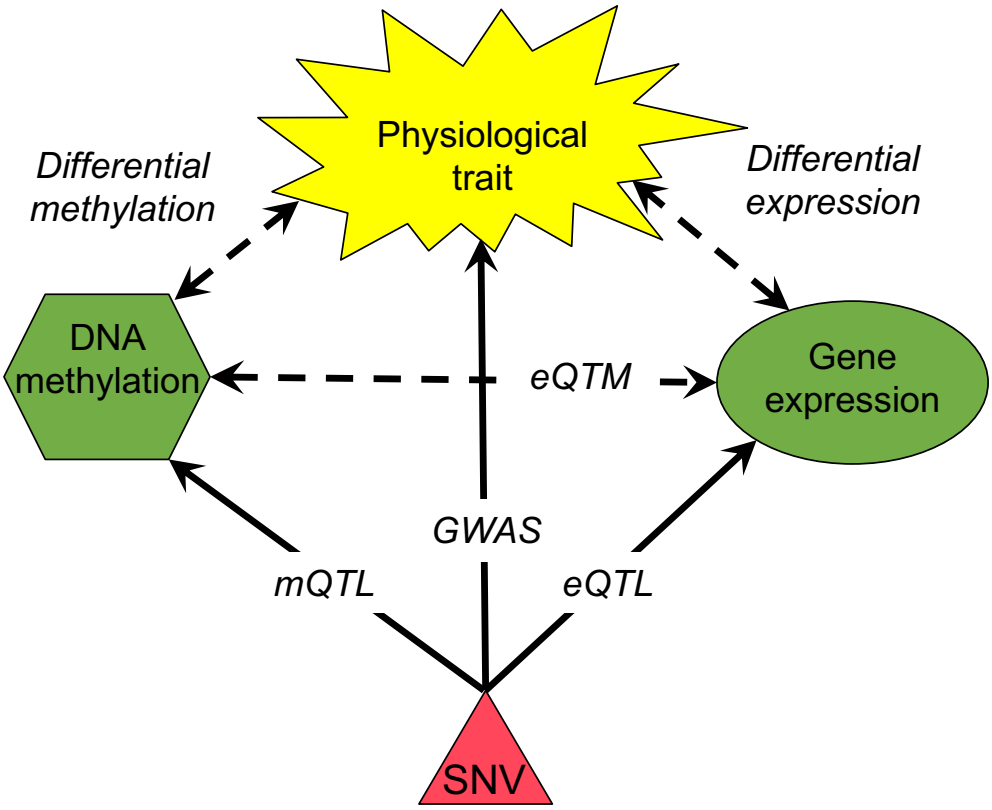

Fig. S1. Schematic overview of the SNV, molecular, and disease/quantitative trait associations and causal relationships assessed in this study. Terms used in figure: single nucleotide variant (SNV), expression quantitative trait locus (eQTL; association between SNV and gene expression), methylation quantitative trait locus (mQTL; association between SNV and DNA methylation), locus from a genome wide association study for a physiological trait (GWAS; association between SNV and a physiological trait), expression quantitative trait methylation (eQTM; association between gene expression and DNA methylation). Solid black lines represent associations where the causal direction is known (could have potential intermediate causal states). Dashed black lines indicate potential causal relationships assessed in this study, where the causal relationship could go in either direction or have an independent source.

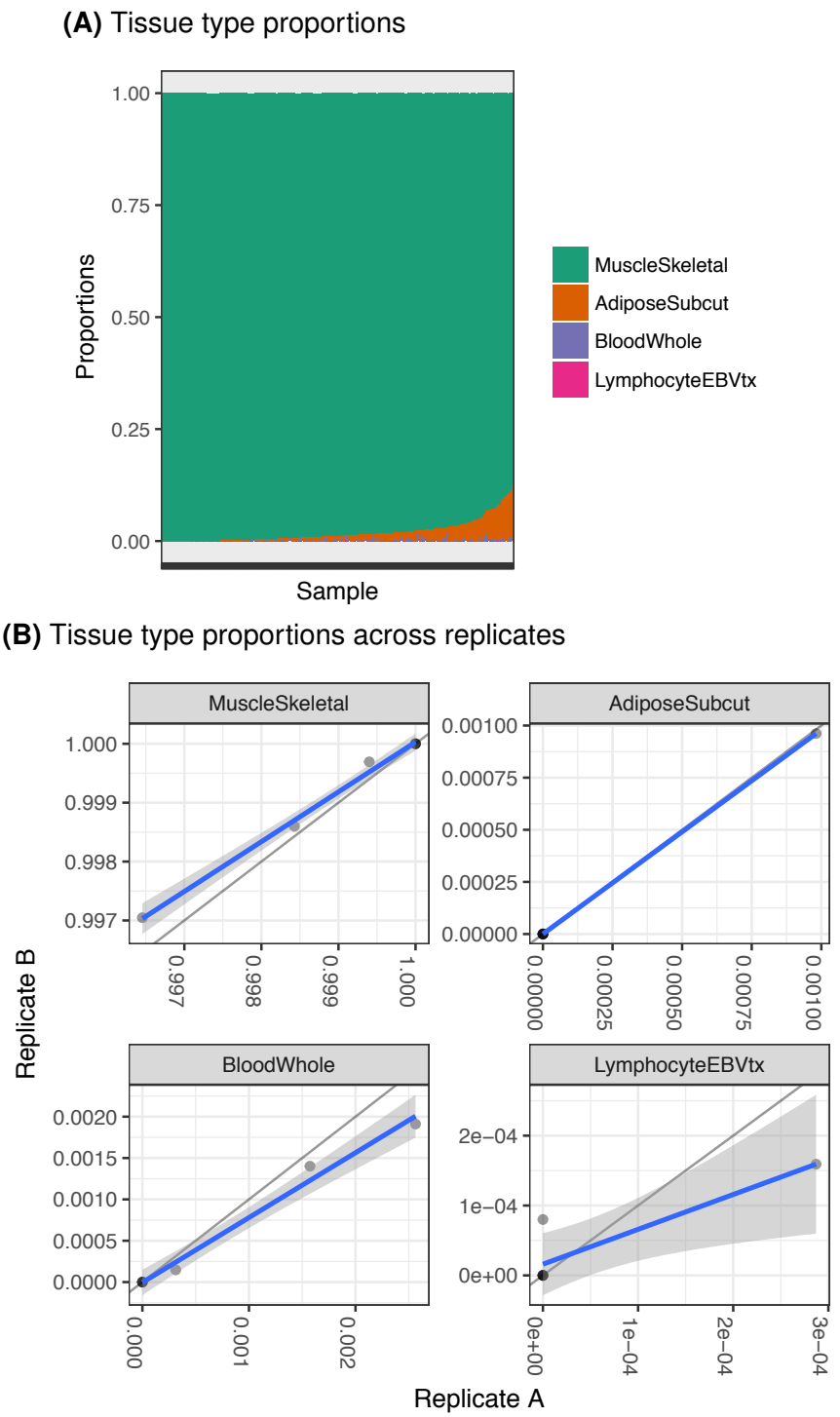

Fig. S2. Estimated tissue type proportions. (A) Tissue fraction estimates using GTEx tissues as a reference. Across the FUSION skeletal muscle samples that passed QC, we estimated 0-12.6% adipose, 0% skin, 0-0.4% lymphocytes, 0-1.8% whole blood, and 87.4-100% skeletal muscle tissue. (B) Comparison of each estimated tissue fraction proportion across six replicate samples with replicates labeled A and B (sample A, x-axis; sample B, y-axis).

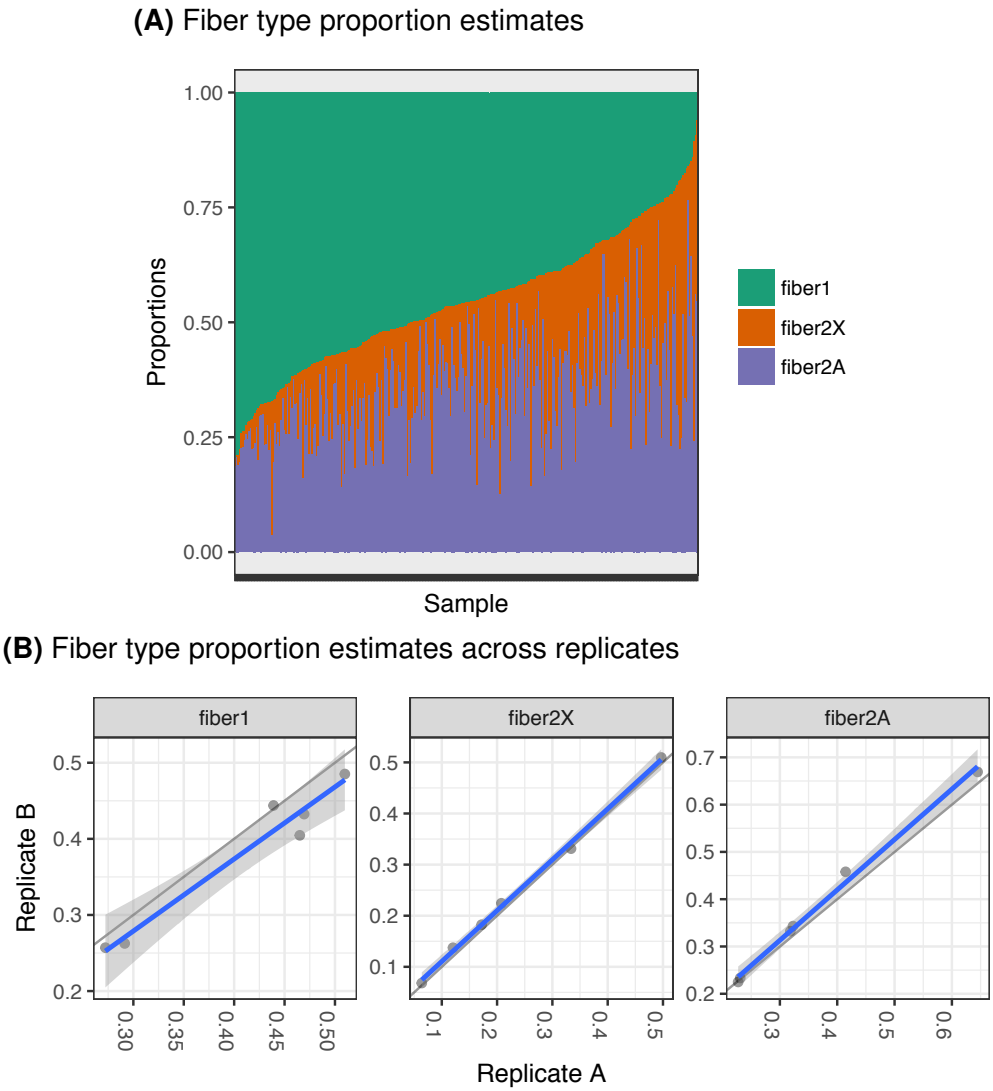

Fig. S3. Estimated fiber type proportions. (A) Estimated fiber type proportions (based on *MYH1*, *MYH2*, and *MYH7* expression). Across the FUSION skeletal muscle samples that passed QC, we estimated 5.9-79.4% type 1, 0.3-65.2% type 2X, and 3.8-76.6% type 2A. (B) Comparison of each estimated tissue fraction proportion across six replicate samples with replicates labeled A and B (sample A, x-axis; sample B, y-axis).

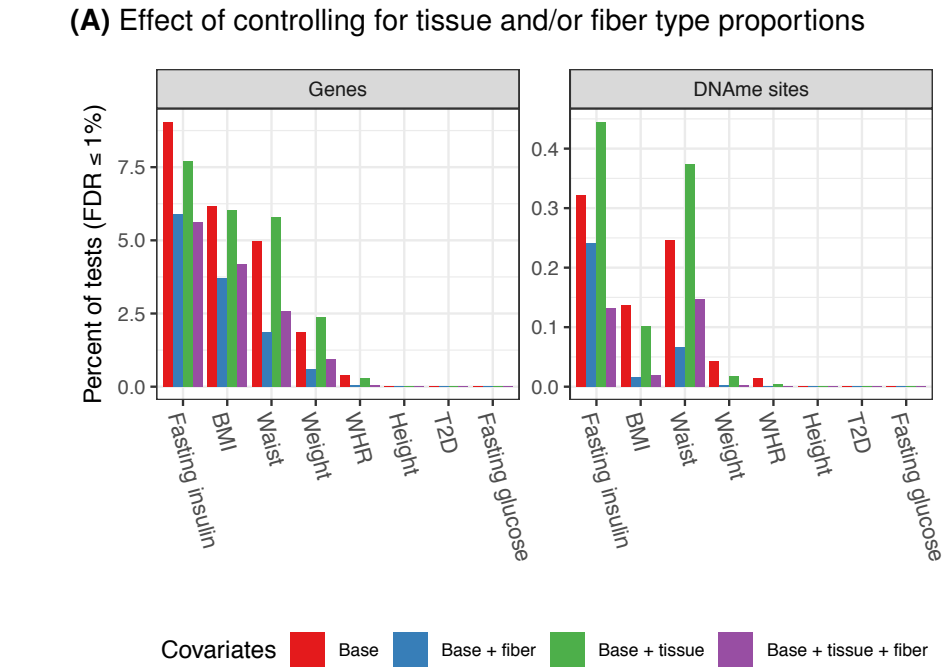

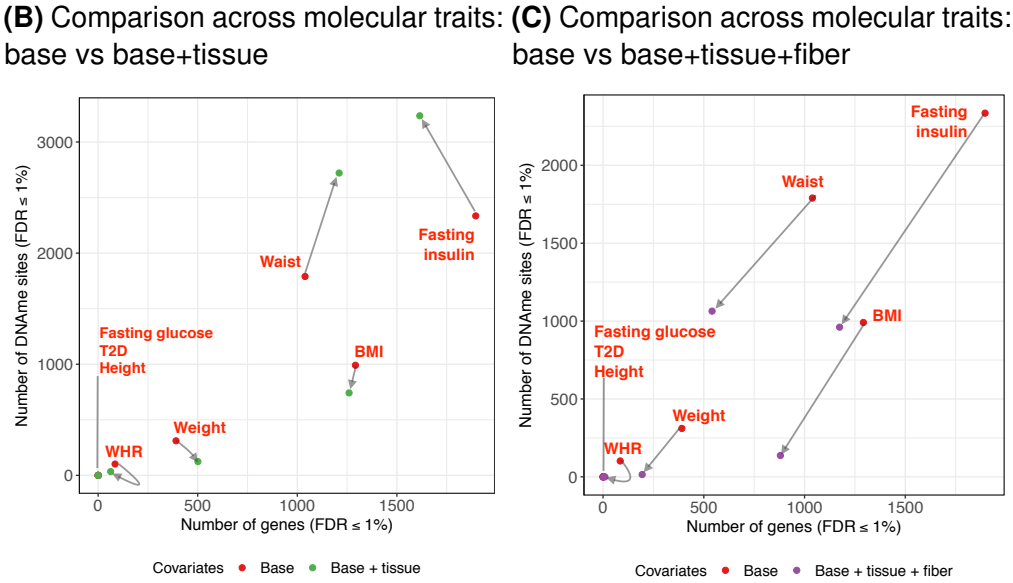

Fig. S4. Association of FUSION physiological traits with skeletal muscle gene expression and DNAme controlling for estimated tissue and/or fiber type proportions. Analysis performed with base covariates (sex, age, sample collection site, smoking status and molecular trait specific technical covariates; "base", red bar and dots), base plus estimated fiber type proportion covariates ("base+fiber", blue bar), base plus estimated tissue type proportion covariates ("base+tissue", green bar and dots) and base plus estimated tissue type proportion and estimated fiber type covariates ("base+tissue+fiber", purple bar and dots). (A) Percent of genes or DNAme sites (y-axis) associated with each physiological trait (x-axis; FDR$\leq 1\%$). (B) Scatter plot of the number of genes (x-axis) and DNAme sites (y-axis) associated with each physiological trait adjusting for base or for base+tissue covariates (results for a given trait connected with black line). (C) Scatter plot of the number of genes (x-axis) and DNAme sites (y-axis) associated with each physiological trait adjusting for base or for base+tissue+fiber covariates (results for a given trait connected with black line).

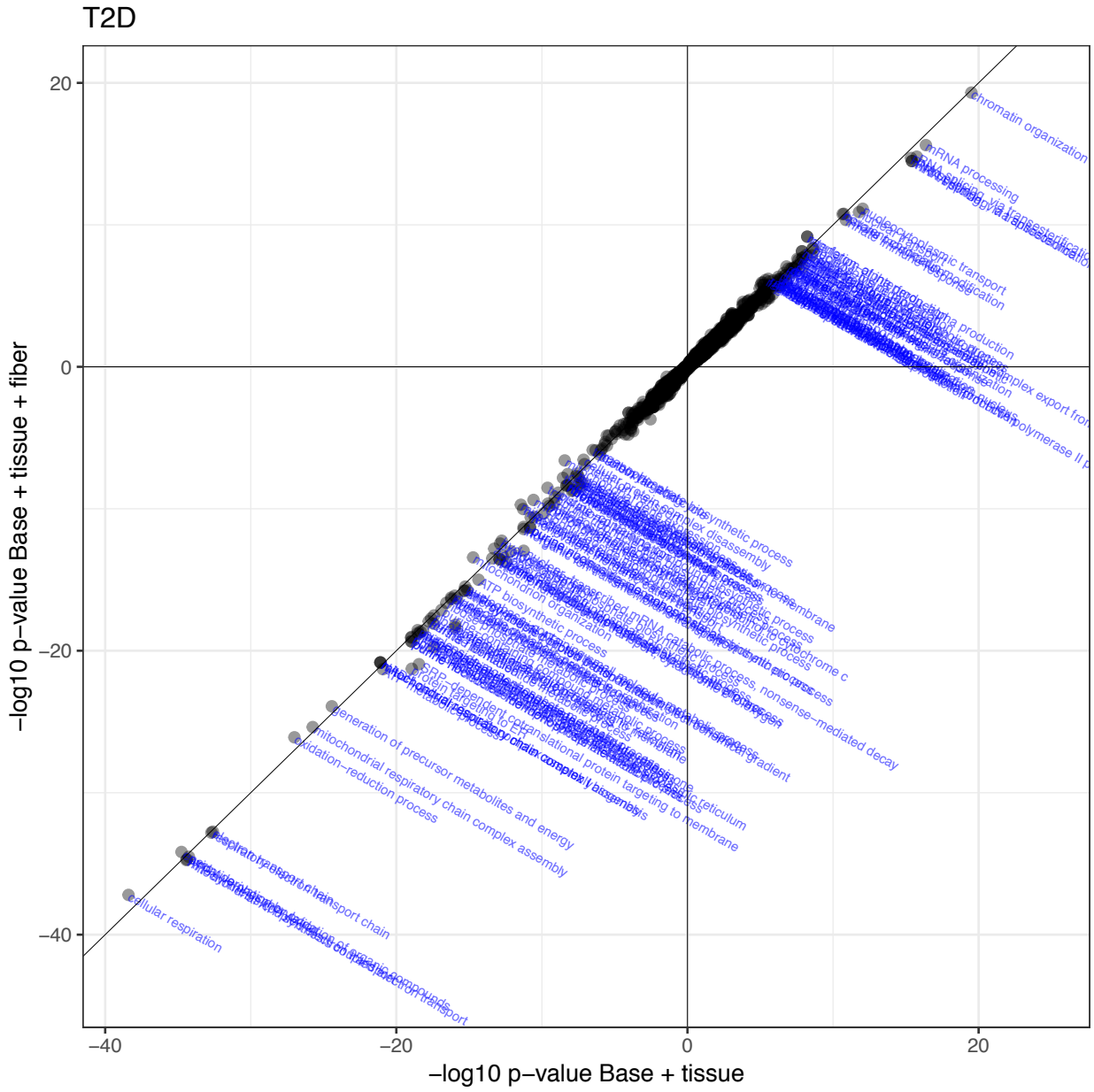

Fig. S5. Effect of including fiber type on physiological trait-gene expression analysis based GO terms: type 2 diabetes status. Scatter plots of $-\log_{10}(p)$ for GO term analysis of the results of association analysis between physiological traits (by page, fasting insulin, BMI, waist, weight, WHR, height, T2D) with gene expression adjusting for base+tissue covariates (x-axis) or base+tissue+fiber covariates (y-axis; covariates as defined in Fig. 1). Identity line in black.

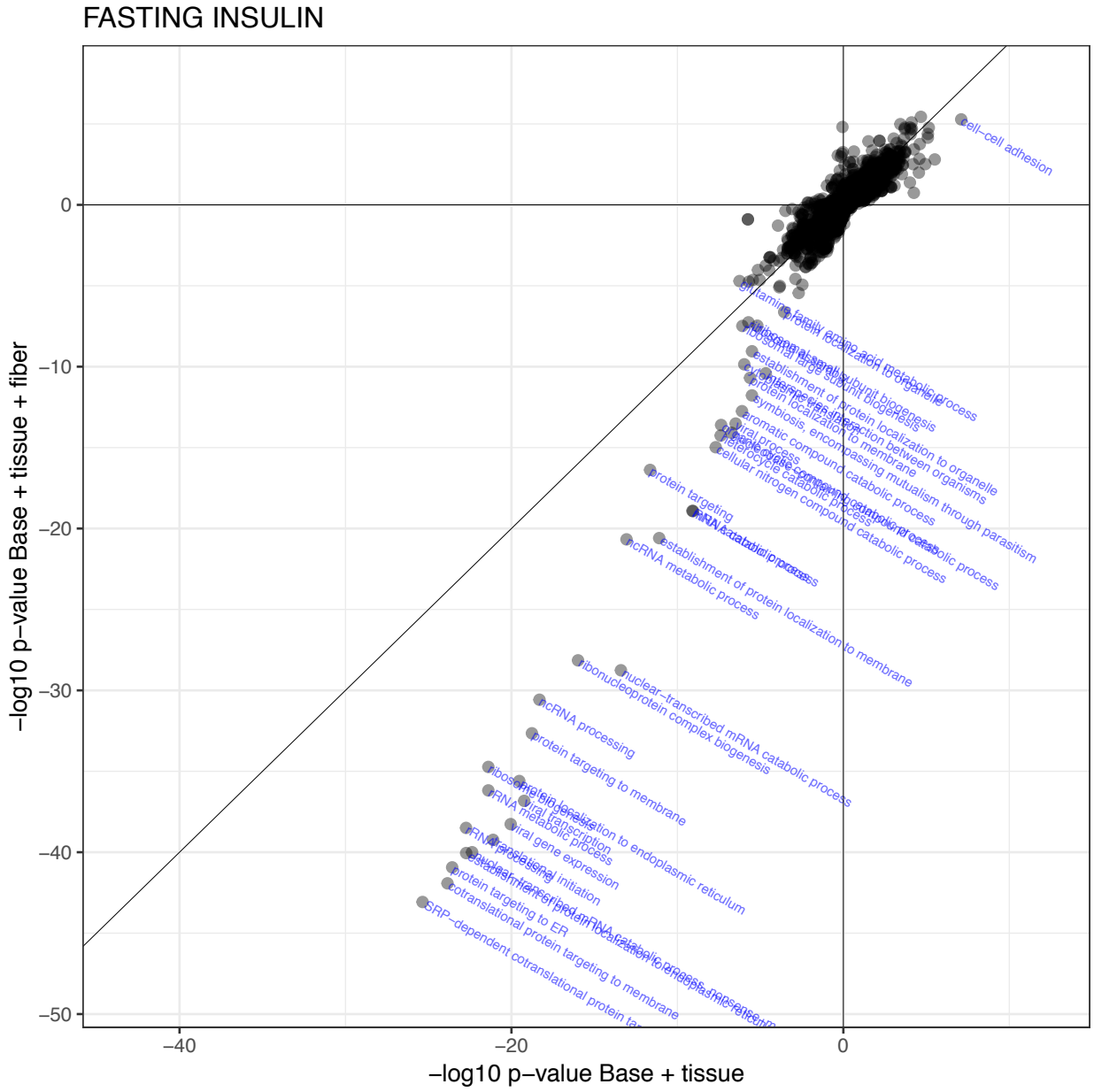

Fig. S6. Effect of including fiber type on physiological trait-gene expression analysis based GO terms: fasting insulin. Scatter plots of $-\log_{10}(p)$ for GO term analysis of the results of association analysis between physiological traits (by page, fasting insulin, BMI, waist, weight, WHR, height, T2D) with gene expression adjusting for base+tissue covariates (x-axis) or base+tissue+fiber covariates (y-axis; covariates as defined in Fig. 1). Identity line in black.

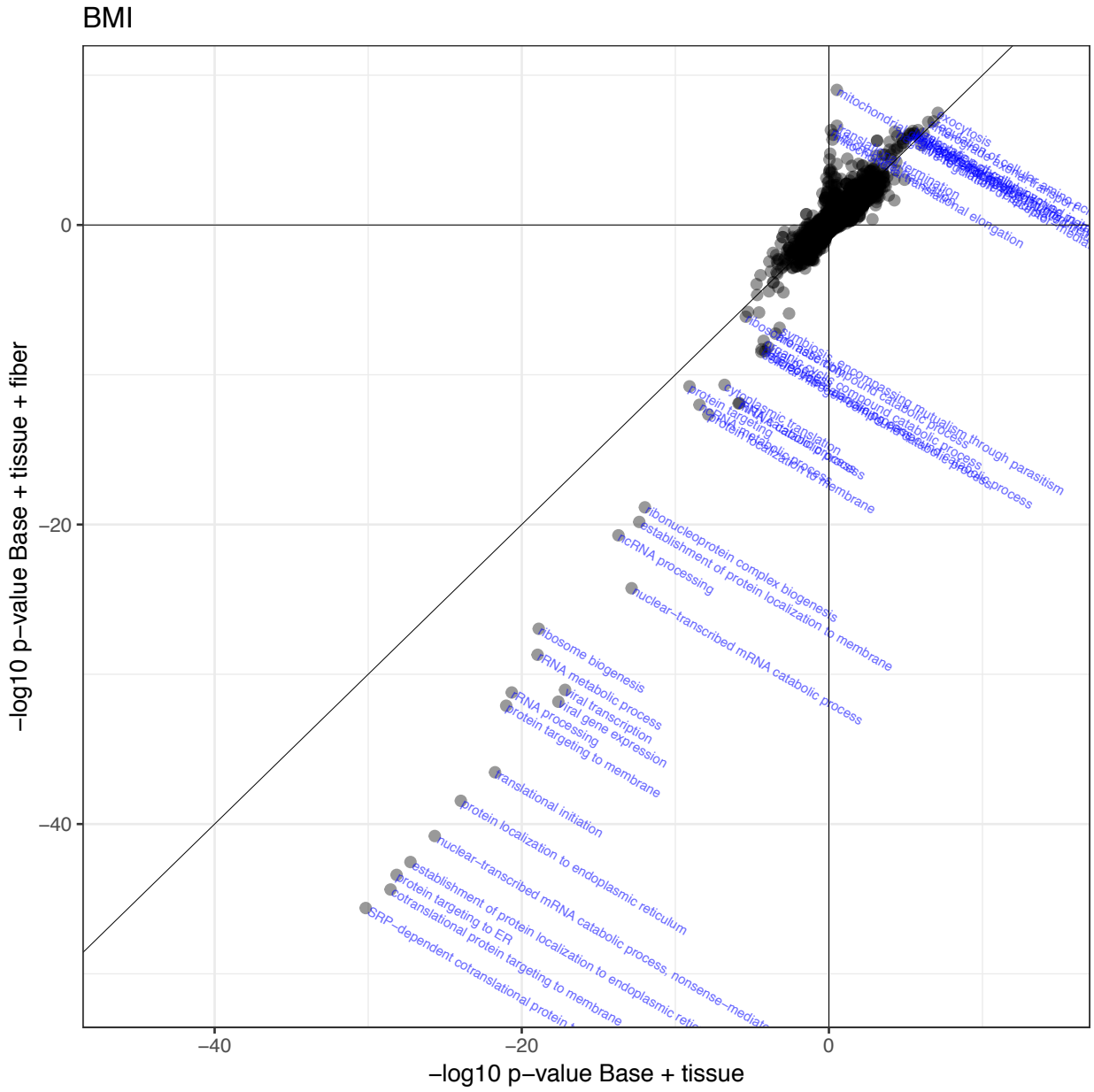

Fig. S7. Effect of including fiber type on physiological trait-gene expression analysis based GO terms: body mass index. Scatter plots of $-\log_{10}(p)$ for GO term analysis of the results of association analysis between physiological traits (by page, fasting insulin, BMI, waist, weight, WHR, height, T2D) with gene expression adjusting for base+tissue covariates (x-axis) or base+tissue+fiber covariates (y-axis; covariates as defined in Fig. 1). Identity line in black.

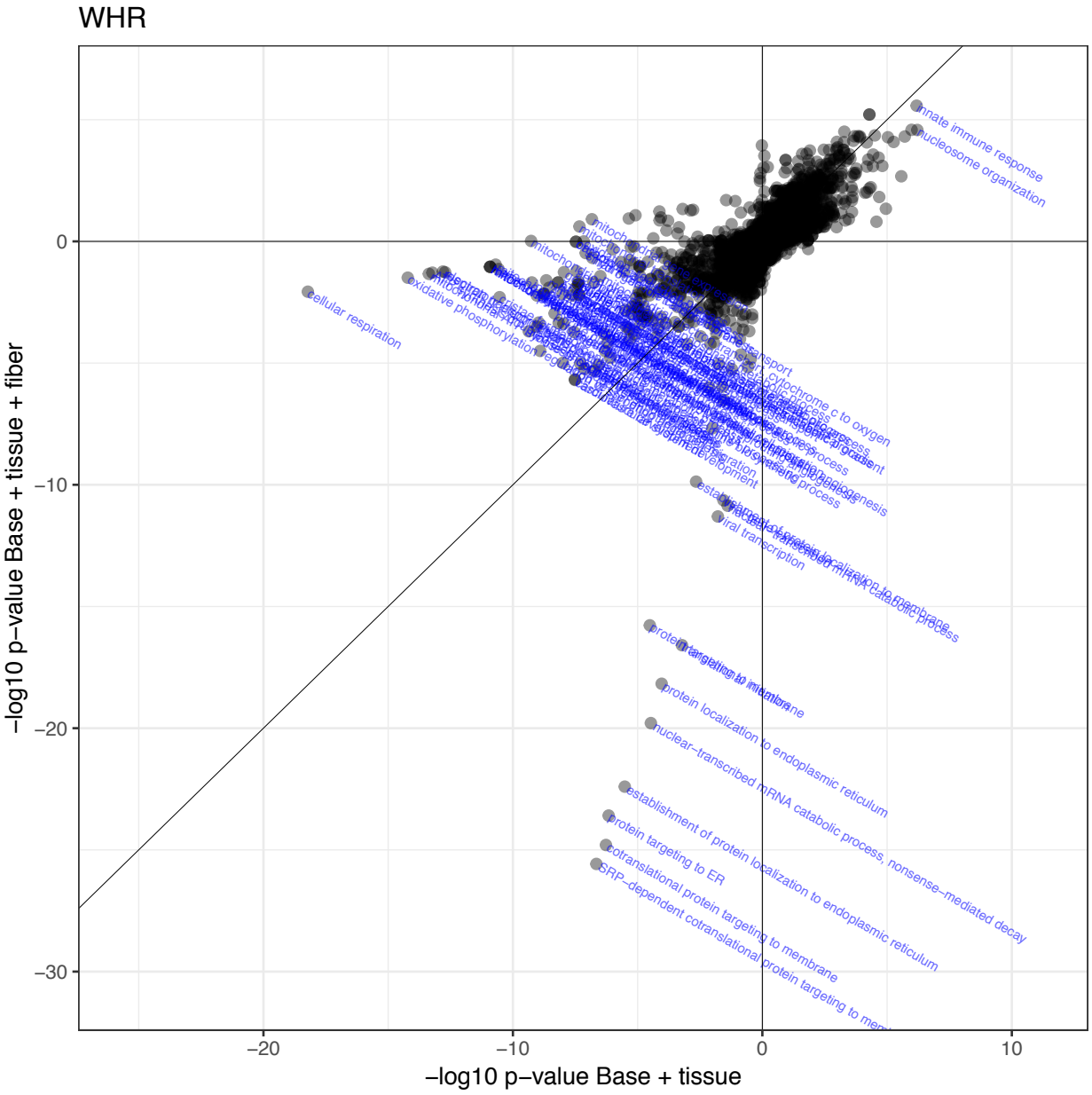

Fig. S8. Effect of including fiber type on physiological trait-gene expression analysis based GO terms: waist hip ratio. Scatter plots of $-\log_{10}(p)$ for GO term analysis of the results of association analysis between physiological traits (by page, fasting insulin, BMI, waist, weight, WHR, height, T2D) with gene expression adjusting for base+tissue covariates (x-axis) or base+tissue+fiber covariates (y-axis; covariates as defined in Fig. 1). Identity line in black.

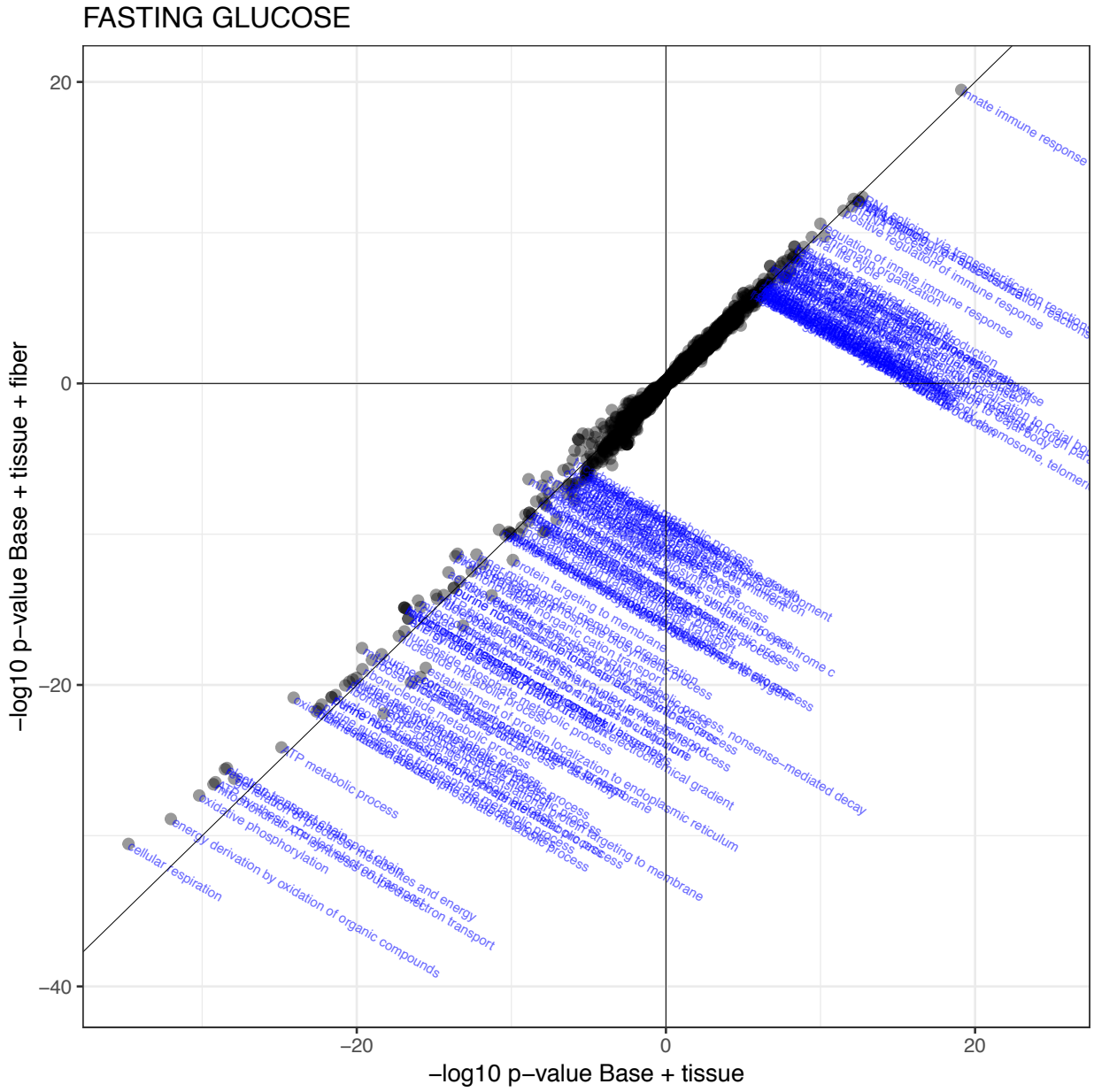

Fig. S9. Effect of including fiber type on physiological trait-gene expression analysis based GO terms: fasting glucose. Scatter plots of $-\log_{10}(p)$ for GO term analysis of the results of association analysis between physiological traits (by page, fasting insulin, BMI, waist, weight, WHR, height, T2D) with gene expression adjusting for base+tissue covariates (x-axis) or base+tissue+fiber covariates (y-axis; covariates as defined in Fig. 1). Identity line in black.

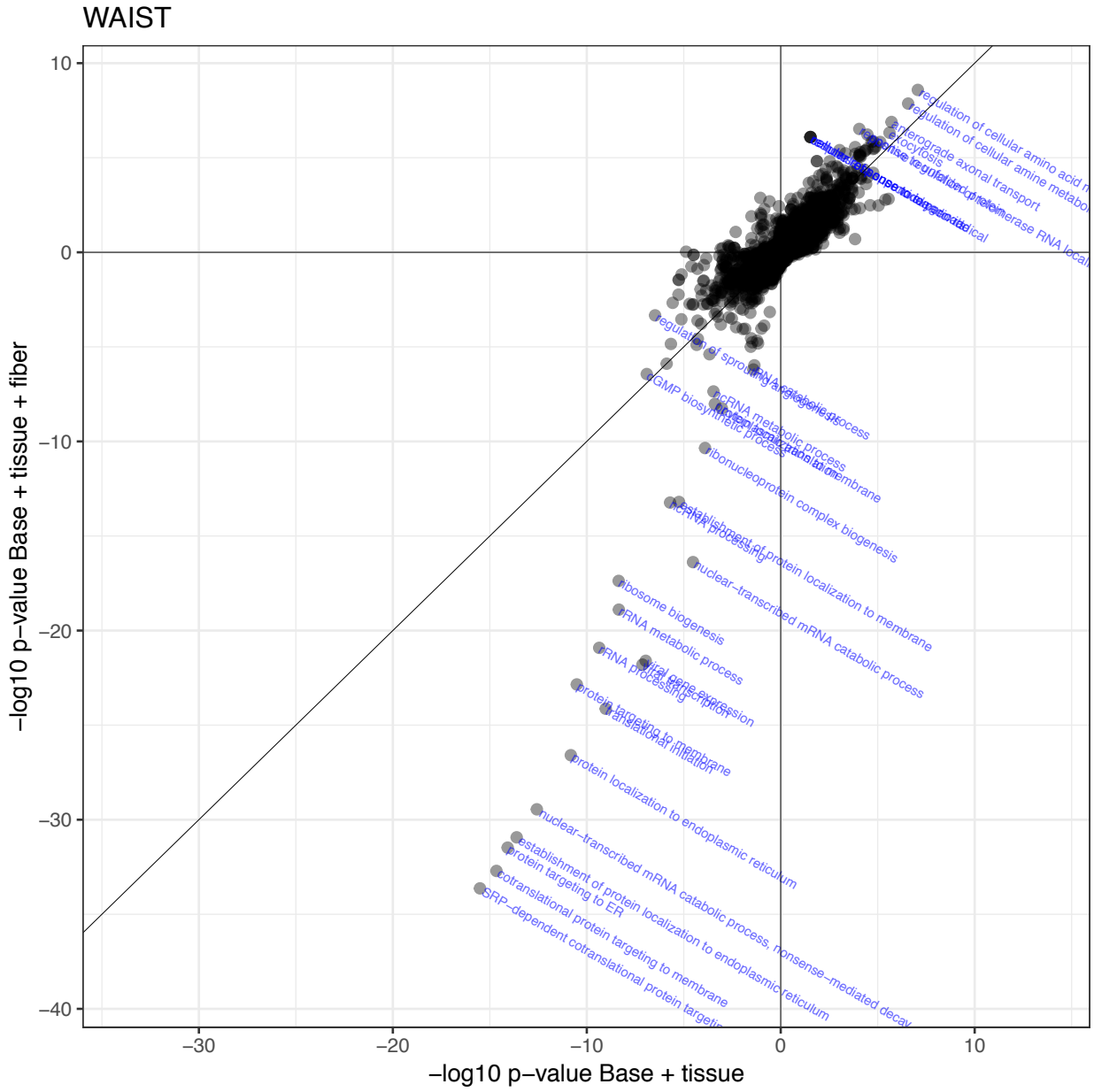

Fig. S10. Effect of including fiber type on physiological trait-gene expression analysis based GO terms: waist. Scatter plots of $-\log_{10}(p)$ for GO term analysis of the results of association analysis between physiological traits (by page, fasting insulin, BMI, waist, weight, WHR, height, T2D) with gene expression adjusting for base+tissue covariates (x-axis) or base+tissue+fiber covariates (y-axis; covariates as defined in Fig. 1). Identity line in black.

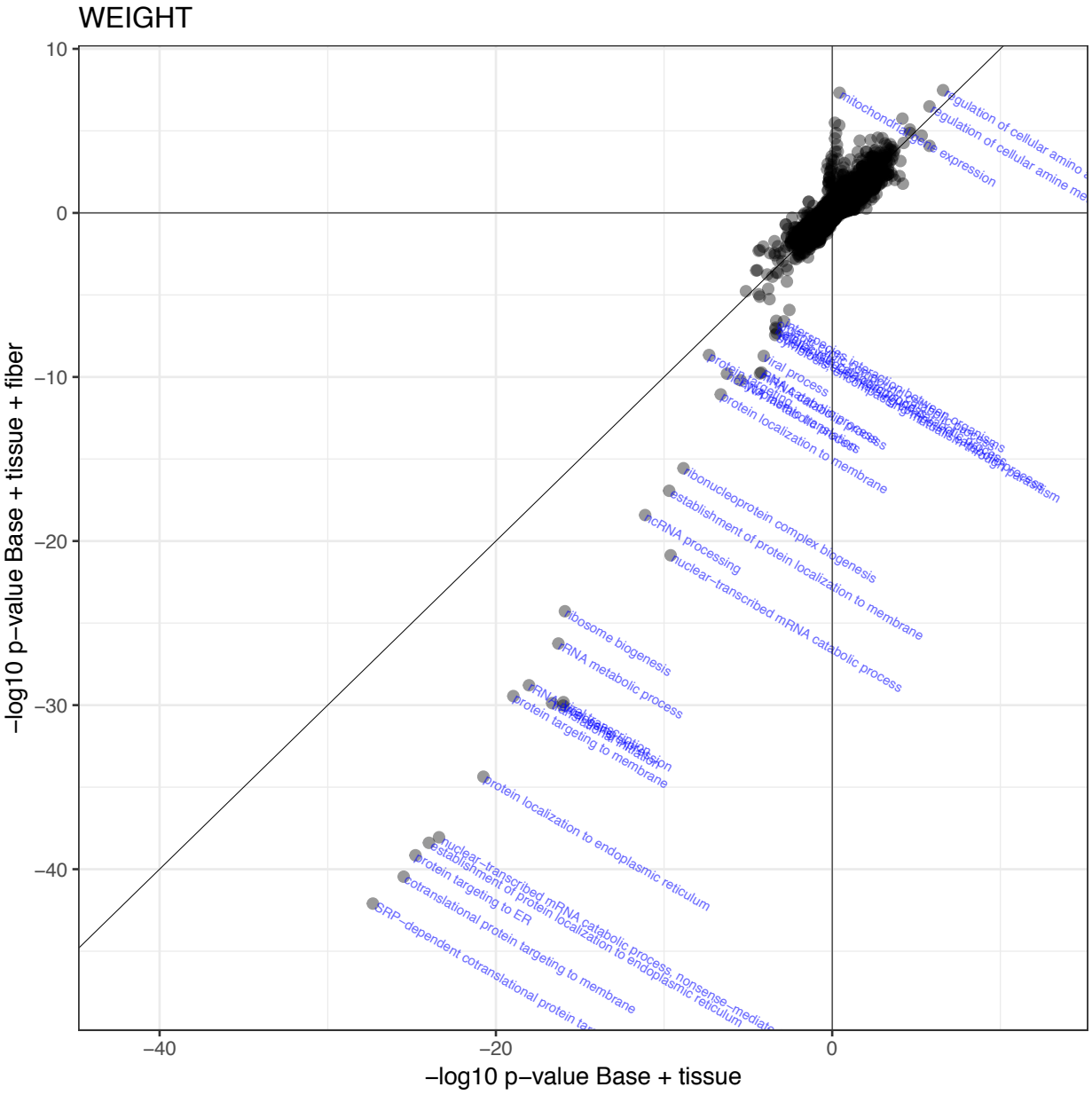

Fig. S11. Effect of including fiber type on physiological trait-gene expression analysis based GO terms: weight. Scatter plots of $-\log_{10}(p)$ for GO term analysis of the results of association analysis between physiological traits (by page, fasting insulin, BMI, waist, weight, WHR, height, T2D) with gene expression adjusting for base+tissue covariates (x-axis) or base+tissue+fiber covariates (y-axis; covariates as defined in Fig. 1). Identity line in black.

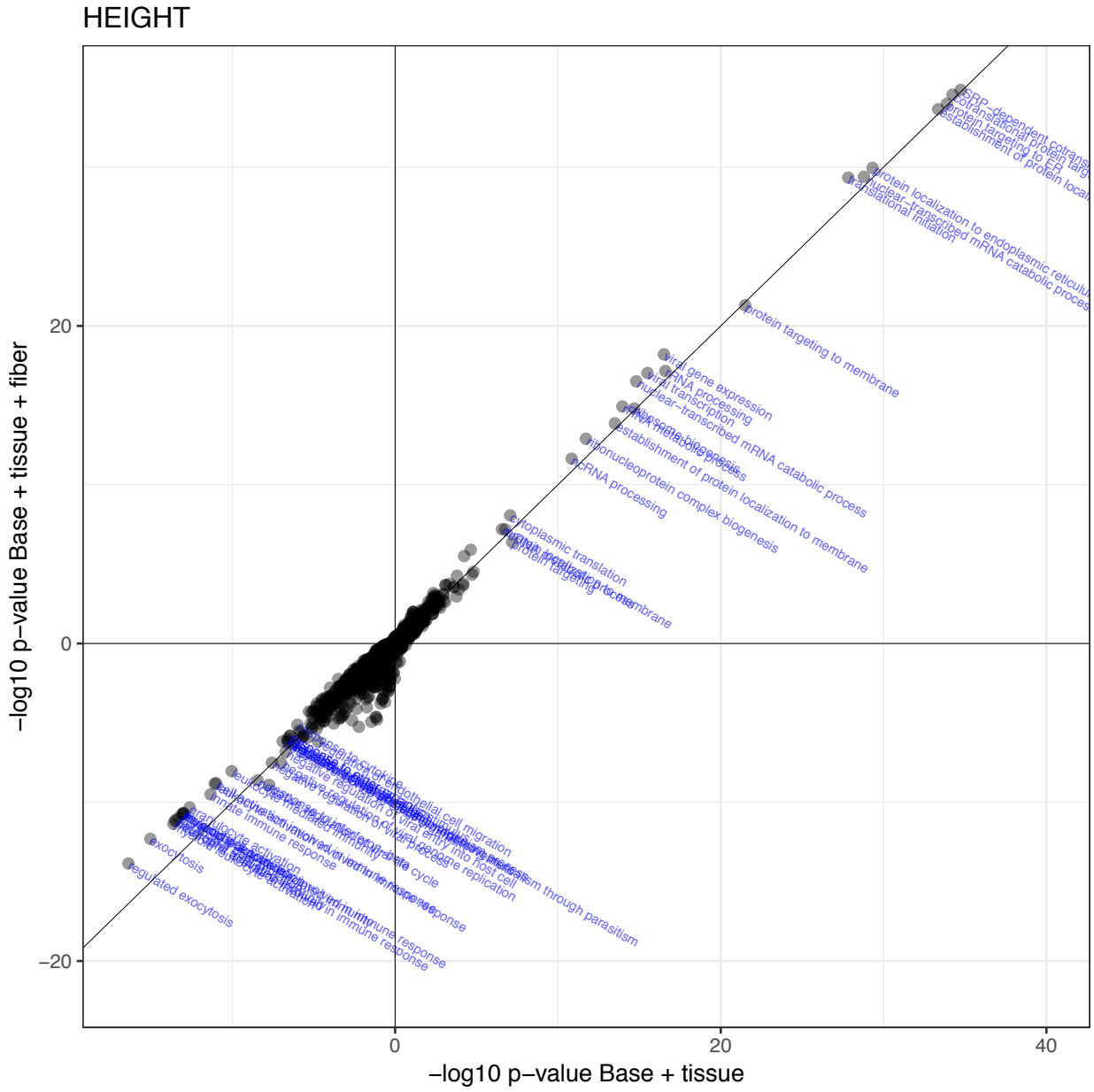

Fig. S12. Effect of including fiber type on physiological trait-gene expression analysis based GO terms: height. Scatter plots of $-\log_{10}(p)$ for GO term analysis of the results of association analysis between physiological traits (by page, fasting insulin, BMI, waist, weight, WHR, height, T2D) with gene expression adjusting for base+tissue covariates (x-axis) or base+tissue+fiber covariates (y-axis; covariates as defined in Fig. 1). Identity line in black.

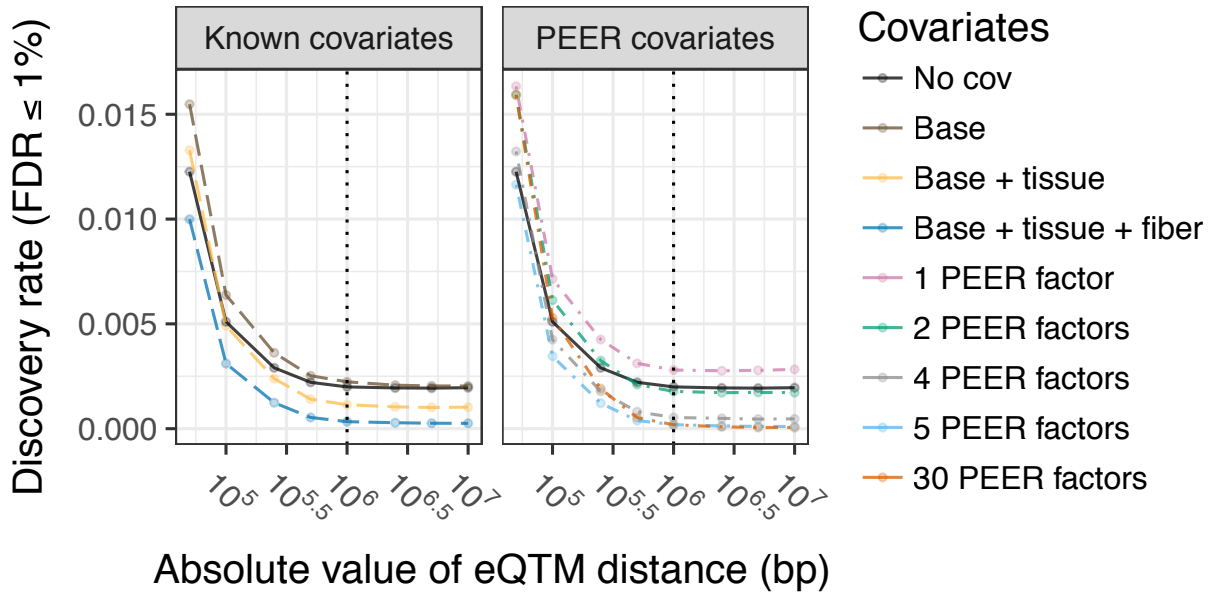

Fig. S13. eQTMs discovered by TSS to DNAme site distance and by method of adjustment for latent factors. Rate of eQTM discovery (y-axis; overall FDR$\leq 1\%$) by distance from eQTM DNAme site to gene TSS distance (x-axis values are the mean distance per bin; Methods). Results adjusted for known covariates (Known covariates panel) or stated number of expression/DNAme PEER factors (PEER covariates panel). We find similar rates of eQTM discovery at DNAme site-TSS distance $>$ 1Mb with adjustments for 5 expression/DNAme PEER factors as for estimated tissue and fiber type (compare blue lines in Known covariates and PEER covariates panels).

(A) eQTM discovery rate binned axis

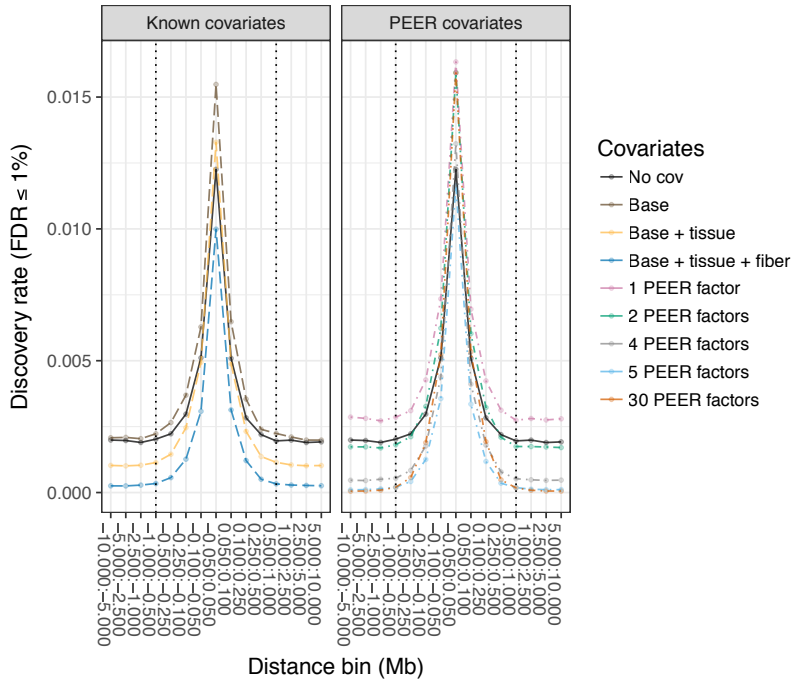

(B) eQTM discovery rate binned axis expanded

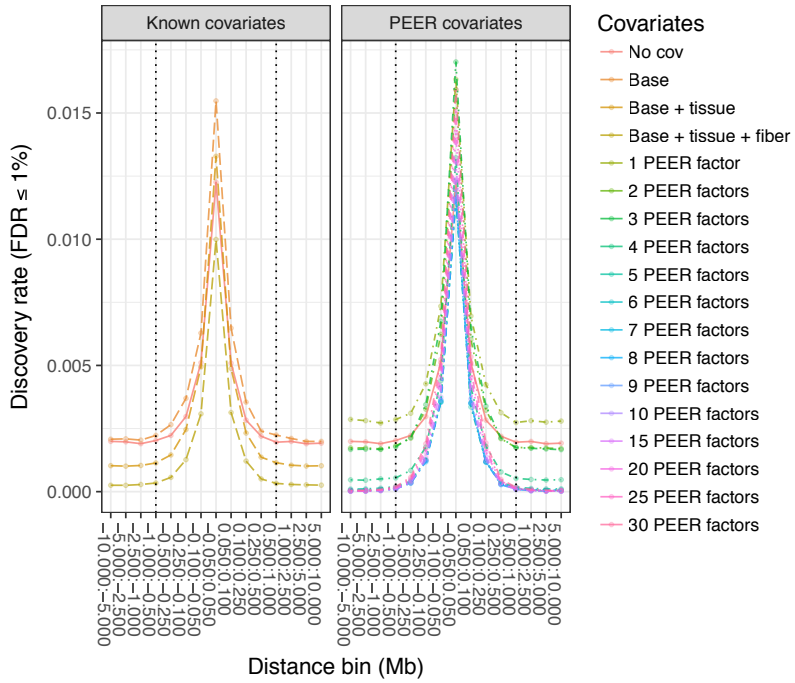

Fig. S14. eQTMs discovered by TSS to DNAme site distance and by method of adjustment for latent factors. (A) Rate of eQTM discovery (y-axis; overall FDR$\leq 1\%$) by DNAme site-TSS distance bin (x-axis). Results adjusted for known covariates (Known covariates panel) or stated number of expression/DNAme PEER factors (PEER covariates panel). Dashed lines at 0.5 to 1 Mb bin. (B) As in panel A, but with additional expression/DNAme PEER factors. Dashed lines at 0.5 to 1 Mb bin.

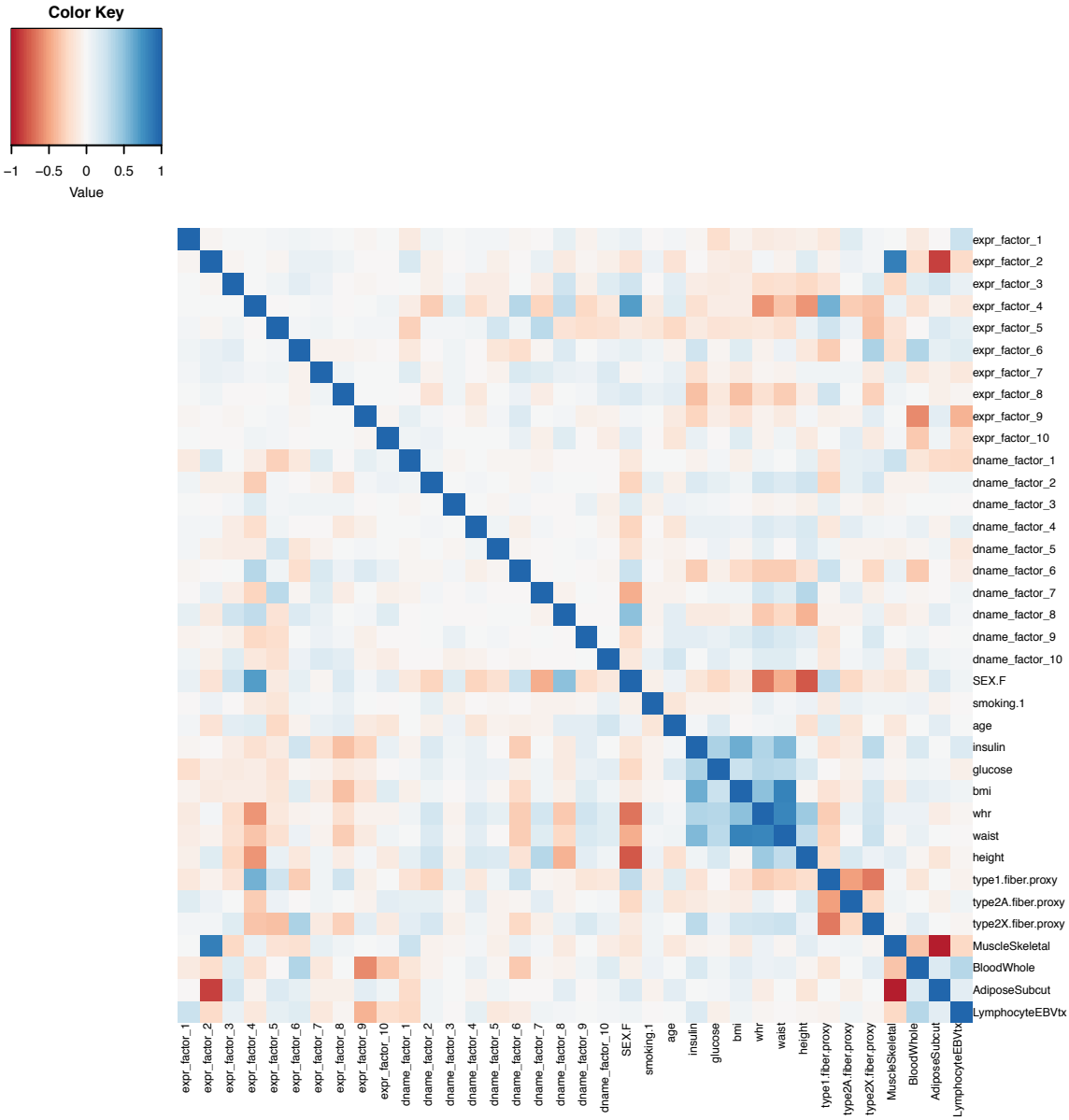

Fig. S15. PEER factor correlation with biological variables. Heatmap of Spearman's rank correlation coefficient (rho) between gene expression PEER factors, DNAme PEER factors, and biological variables. Biological variables include physiological traits, estimated tissue proportion (using GTEx tissues as reference), and estimated muscle fiber type proportions (based on *MYH1*, *MYH2*, and *MYH7* expression).

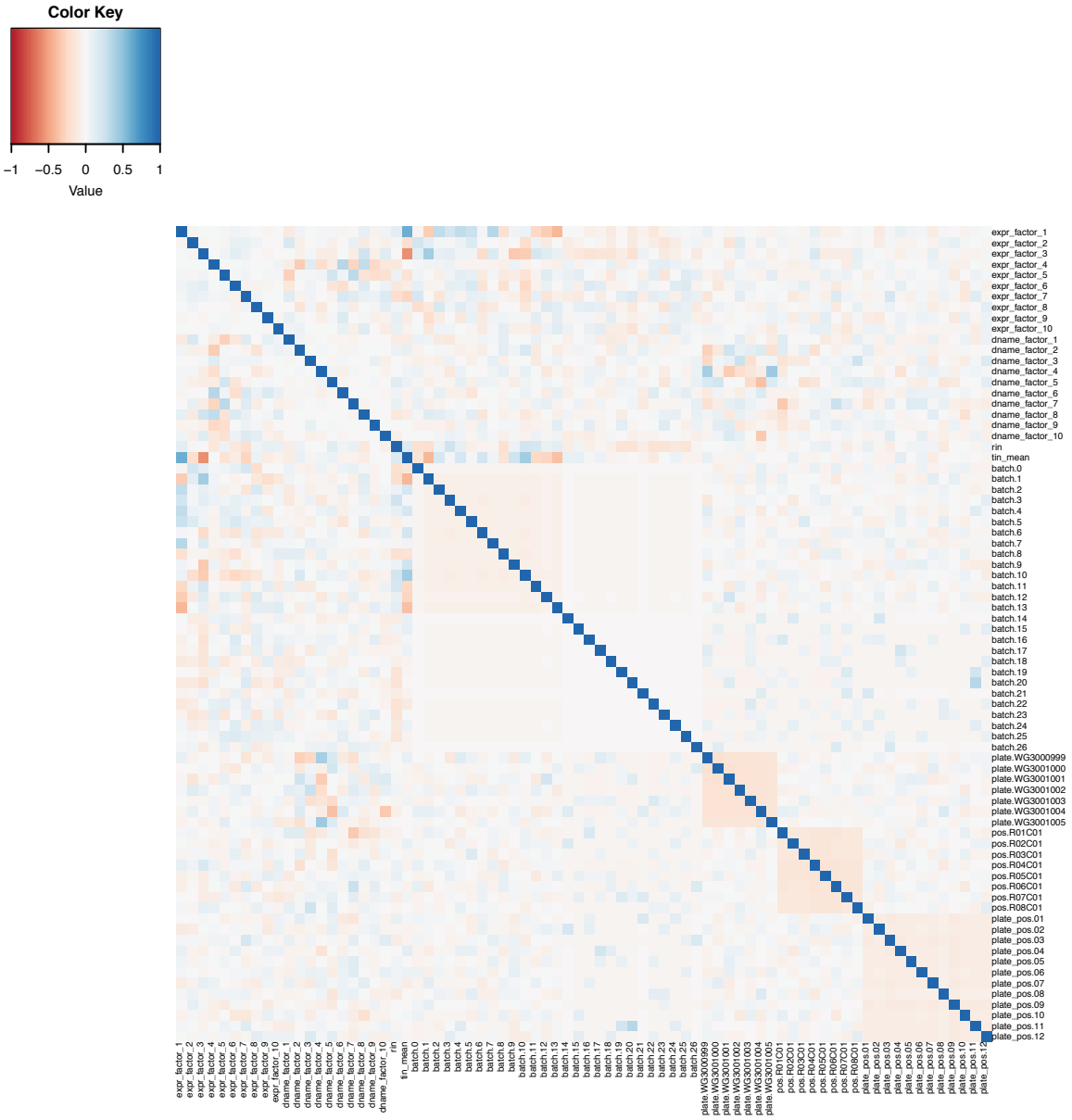

Fig. S16. PEER factor correlation with technical variables. Heatmap of Spearman's rank correlation coefficient (rho) between gene expression PEER factors, DNAme PEER factors, and technical variables. Variables labeled batch* correspond to RNA-sequencing. Variables labeled plate* or pos* correspond to DNAme.

(A) Total genes with an eQTL across PEER factors

(B) Total DNAme sites with an mQTL across PEER factors

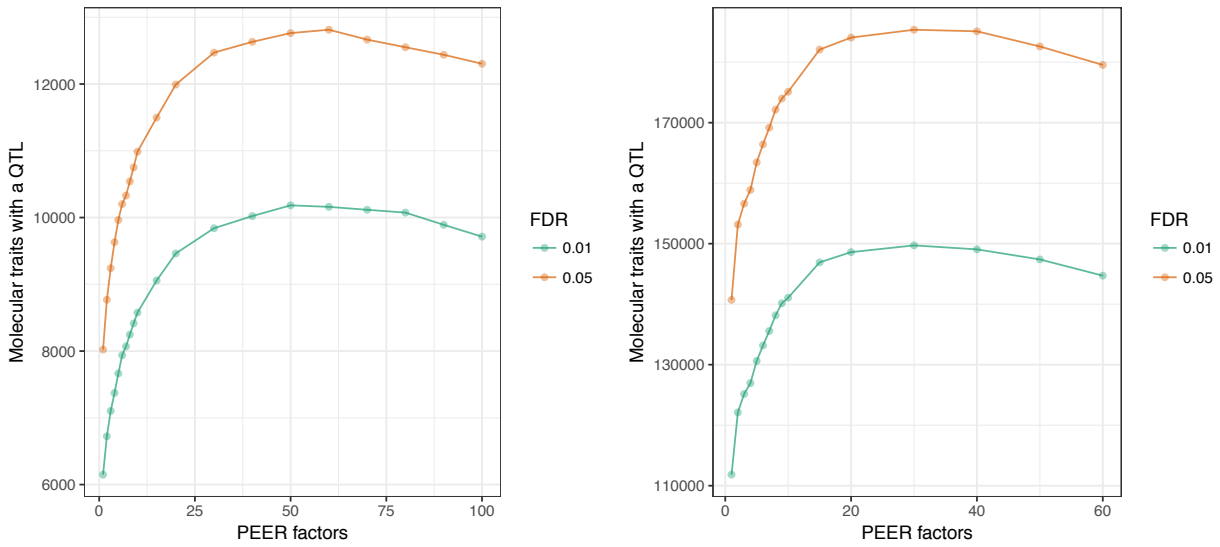

Fig. S17. Comparison of the number of genes and DNAme sites with a QTL and the number of gene expression- and DNAme-based PEER factors included as covariates. (A) Number of genes with an eQTL (y-axis) at FDR$\leq 5\%$(orange line) or FDR$\leq 1\%$ (green line) by the number of expression-based PEER factors included in analysis (x-axis). (B) Number of DNAme sites with an mQTL (y-axis) at FDR$\leq 5\%$ (orange line) or FDR$\leq 1\%$ (green line) by the number of DNAme-based PEER factors included in analysis (x-axis). We selected the number of molecular trait PEER factors that maximized the number genes with an eQTL (50 factors) and DNAme sites with an mQTL (30 factors).

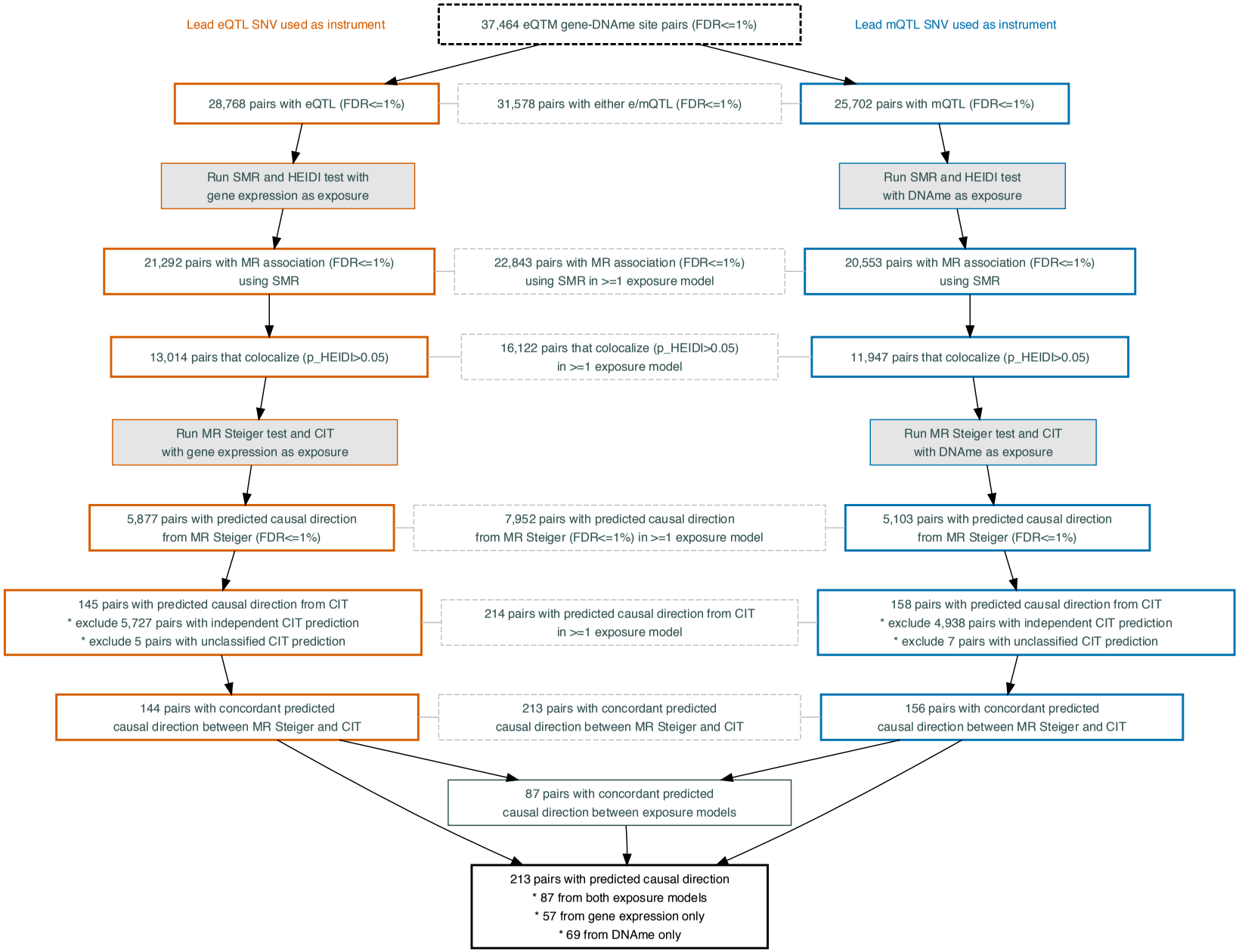

Fig. S18. Workflow of molecular trait Mendelian randomization and causal inference test. Diagram of the workflow used to make causal predictions.

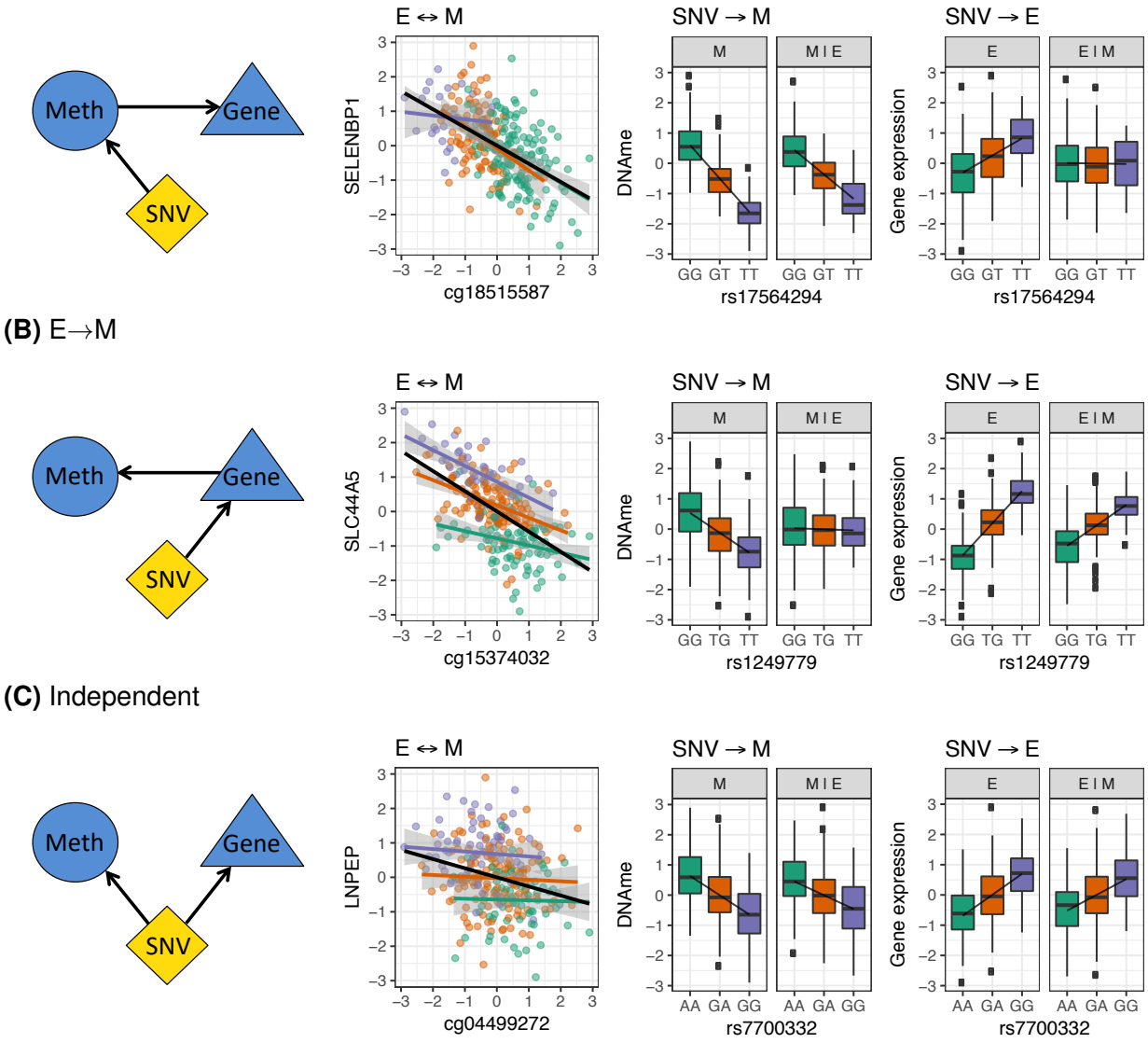

Fig. S19. Examples of molecular mediation. Types of molecular mediation. (A) DNAme→Expression scenario where SNV affects DNAme which changes expression. (B) Expression→DNAme scenario where SNV affects expression which changes DNAme. (C) Independent scenario where the SNV effect on DNAme and expression is independent. For A, B, and C rows: M↔E facet: Scatter plot of residual gene expression (adjusted for PEER factors used in eQTM mapping; y-axis) and residual DNAme (adjusted for PEER factors; x-axis). Linear regression line for eQTM association, overall (black) and colored by the SNV genotype (homozygous genotype, green; heterozygous genotype, orange; other homozygous genotype, purple). SNV→M facet: Box plots and linear regression line (additive model) of residual DNAme by SNV genotype (facet M). Box plot and regression line as for panel M, except with adjustment of residual SNV DNAme by residual gene expression (facet M|E). SNV→E facet: Box plots and linear regression line (additive model) of residual gene expression by SNV genotype (facet E). Box plot and regression line as for panel E except with adjustment of residual gene expression by residual DNAme (facet E|M).

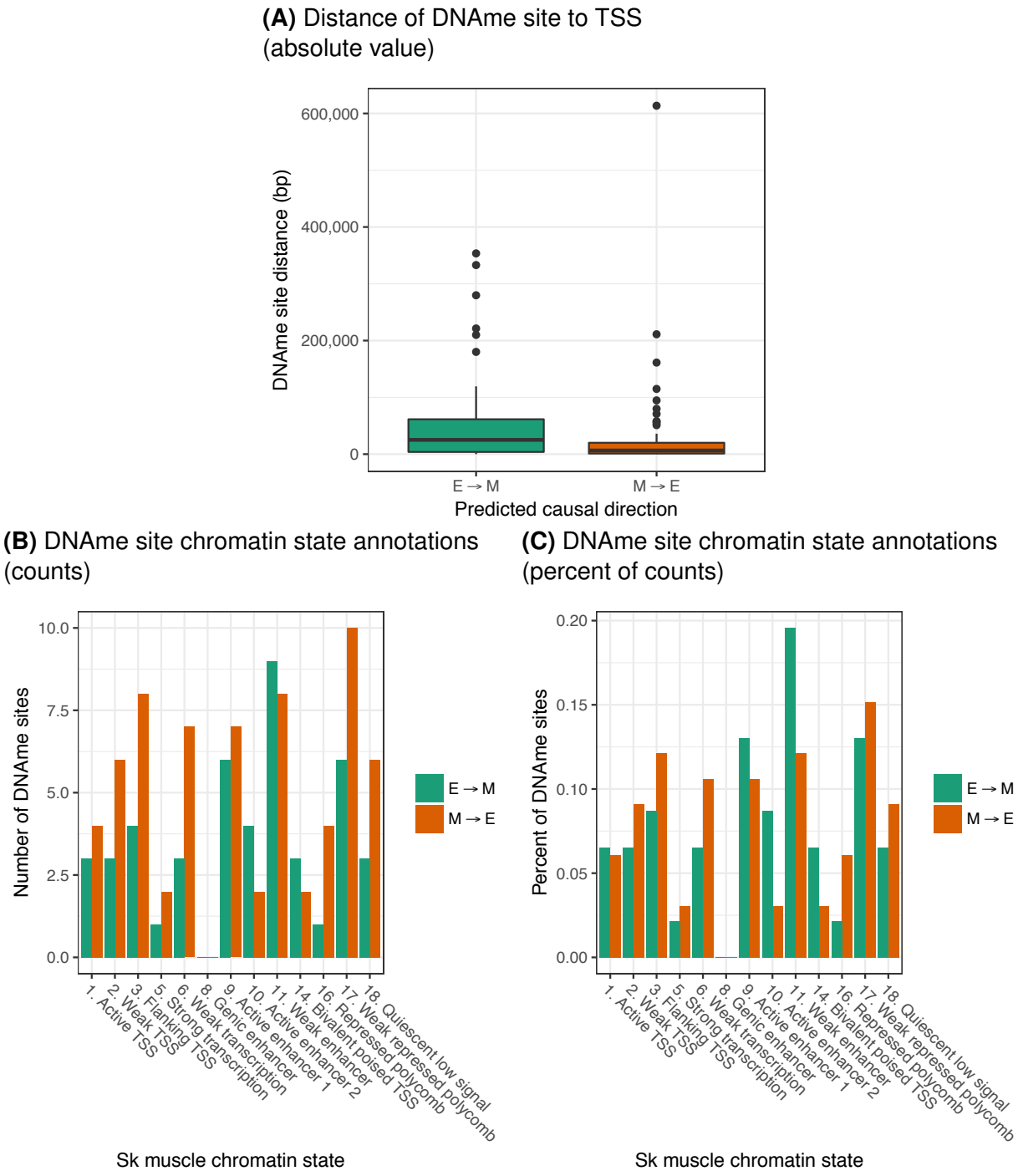

Fig. S20. Comparison of DNAme sites for predicted E→M and M→E causal relationships. We randomly selected a single gene-DNAme site pair for every gene or DNAme site occurring more than once in the data. (A) Box plots of the absolute distance of DNAme site to gene TSS (y-axis) by predicted causal relationship (green E→M, orange M→E). (B) Count of gene-DNAme site pairs (y-axis) by DNAme site skeletal muscle chromatin state annotation and predicted causal relationship (x-axis; green E→M, orange M→E). (C) Percent of gene-DNAme site pairs (y-axis) by DNAme site skeletal muscle chromatin state annotation and predicted causal relationship (x-axis; green E→M, orange M→E).

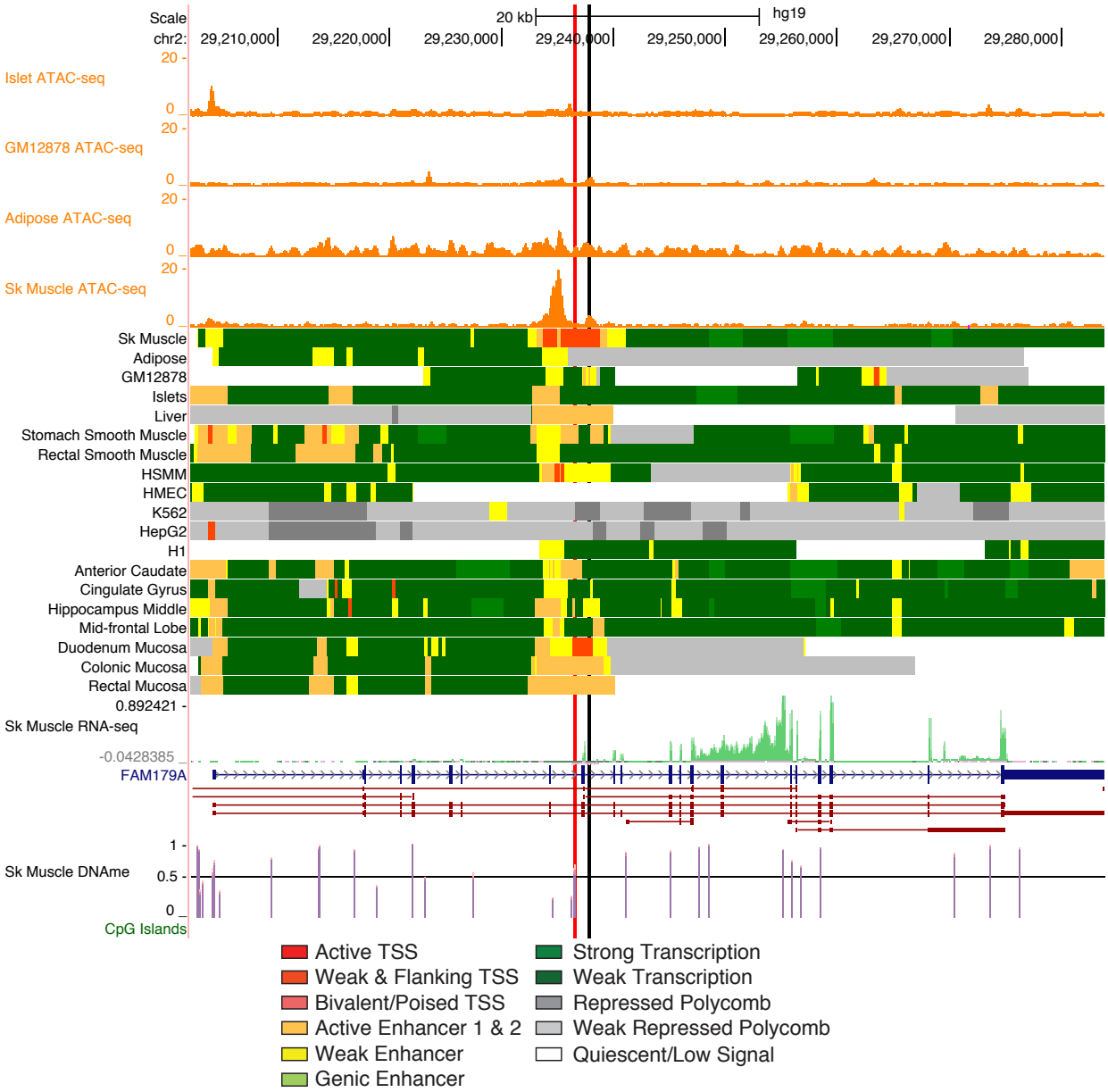

Fig. S21. *FAM179A* locus. ATAC-seq data for four tissues (top orange tracks); chromatin states (tracks with tissue/cell type names); average FUSION skeletal muscle RNA-seq signal (green track); *FAM179A* gene annotation (purple gene structure with red isoforms); average FUSION skeletal muscle DNAme signal (purple bars). Black vertical line at rs1867944. Red vertical line at cg09001591.

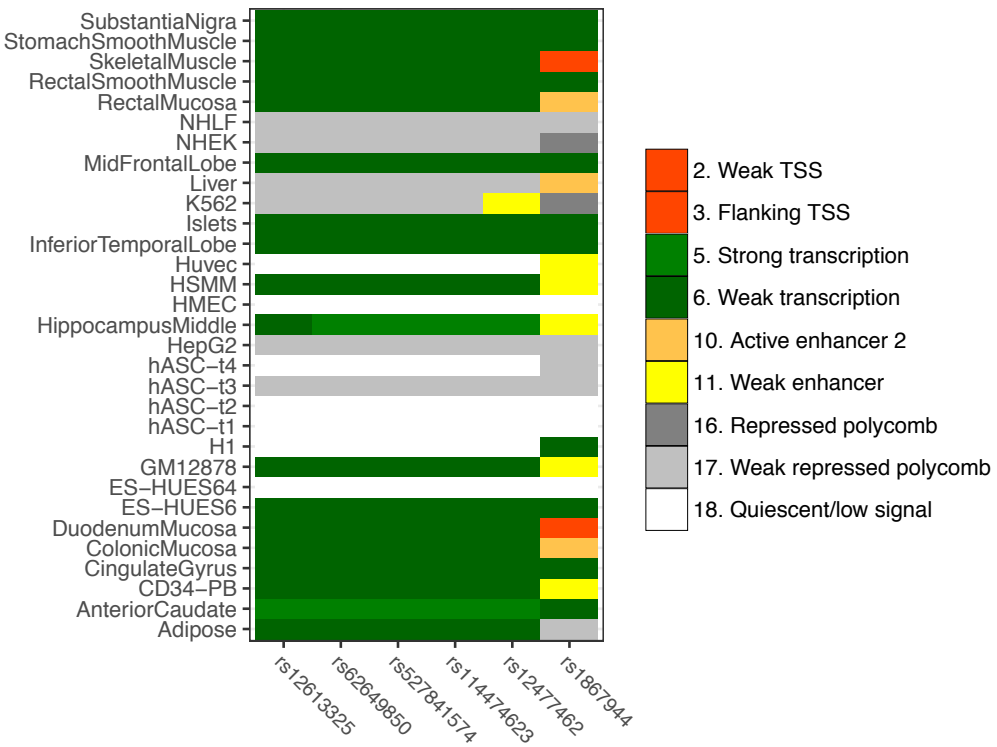

Fig. S22. rs1867944 chromatin states. (A) Tissue/cell type chromatin states at rs1867944 and variants in LD with rs1867944 ($r^2 > 0.8$).

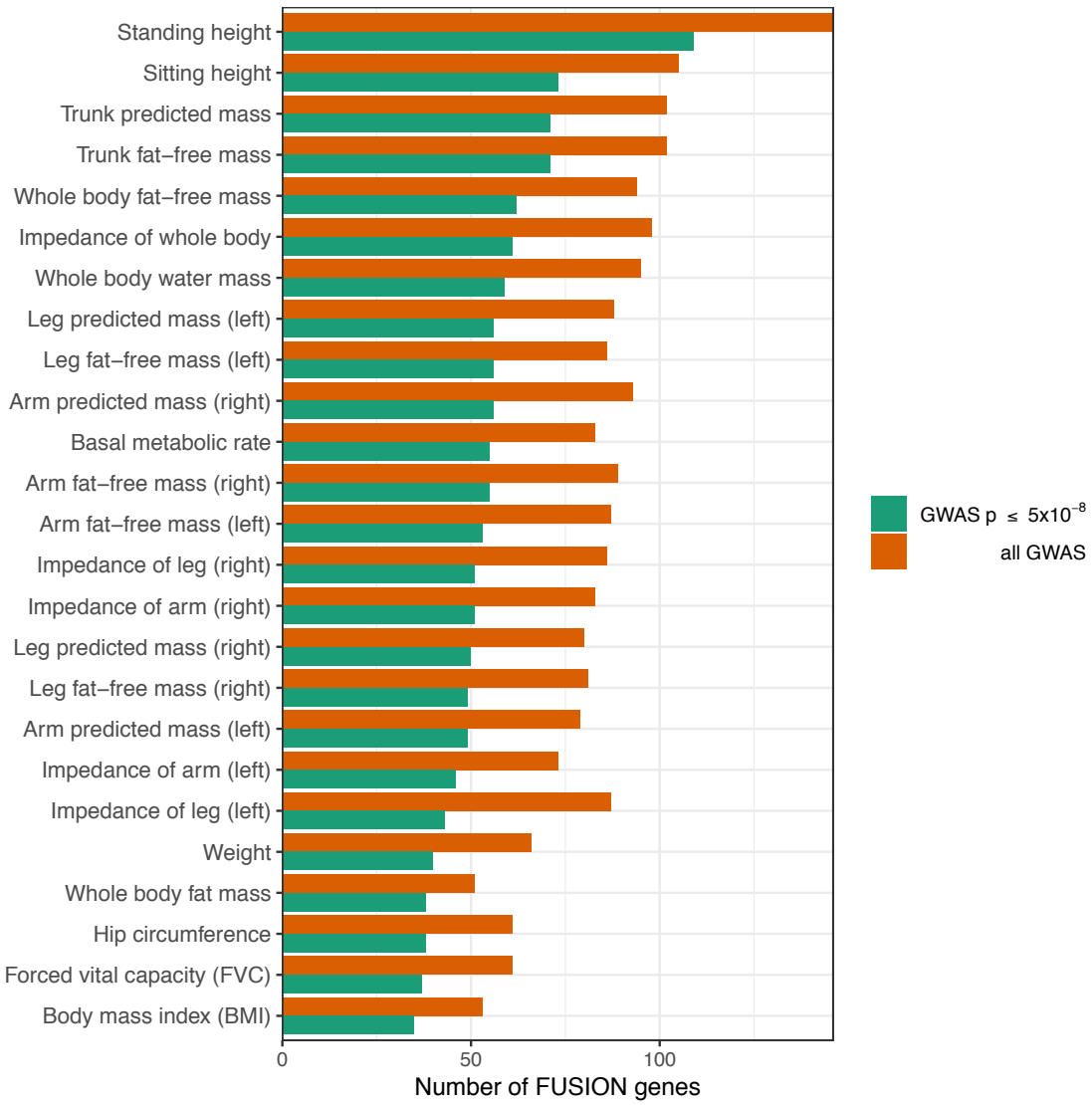

Fig. S23. Number of FUSION gene expression MR associations per disease/quantitative trait. Number of gene-trait pairs (FDR$\leq 1\%$, $p_{\text{HEIDI}} > 0.05$) for each disease/quantitative trait with (green) and without (orange) requiring the top eQTL SNV to have a disease/quantitative trait $p_{\text{GWAS}} \leq 5 * 10^{-8}$. Top 25 disease/quantitative traits shown, full results in Table S7.

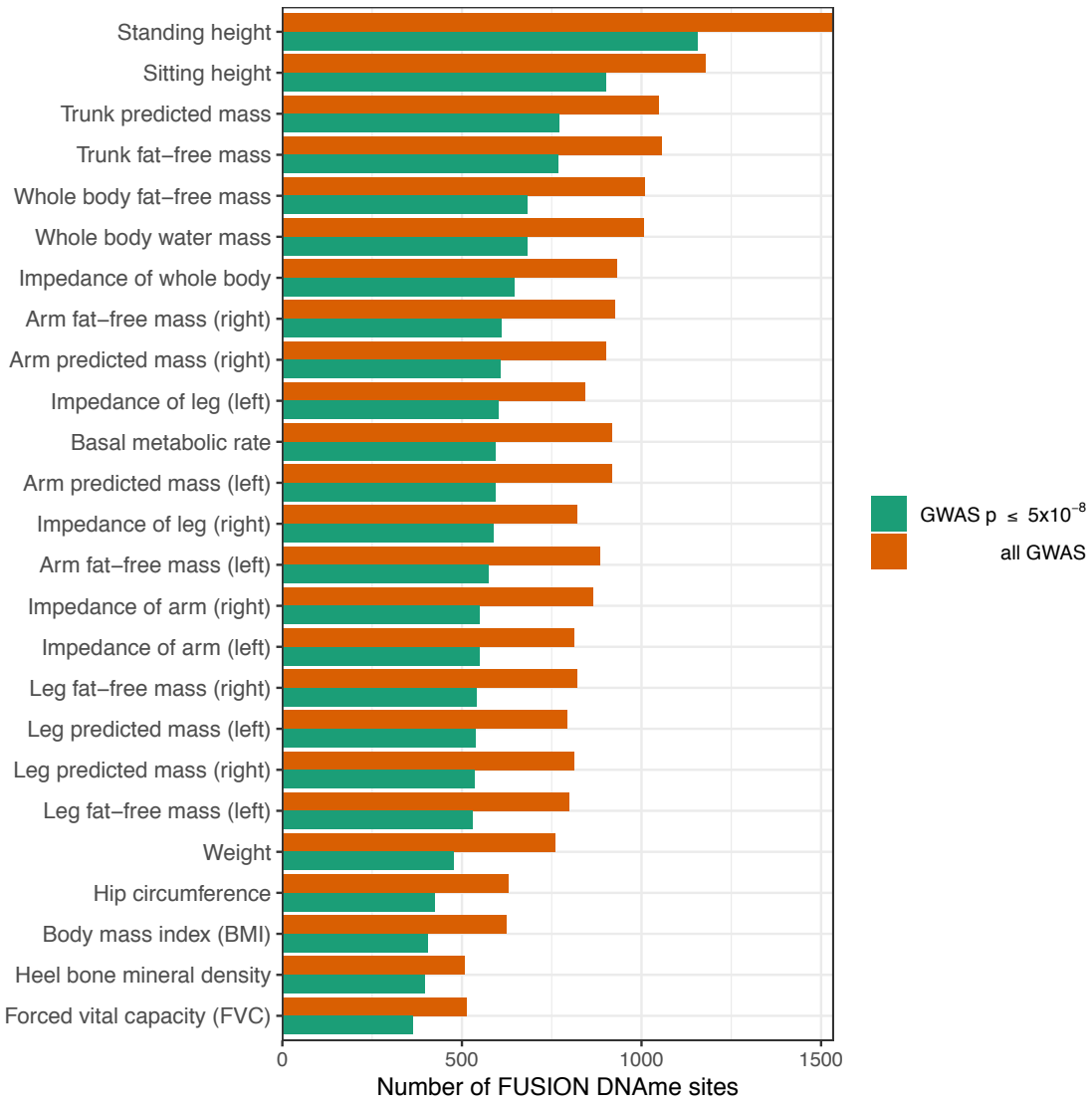

Fig. S24. Number of FUSION DNAme MR associations per disease/quantitative trait. Number of DNAme site-trait pairs (FDR$\leq 1\%$, $p_{\text{HEIDI}} > 0.05$) for each disease/quantitative trait with (green) and without (orange) requiring the top mQTL SNV to have a disease/quantitative trait $p_{\text{GWAS}} \leq 5 * 10^{-8}$. Top 25 disease/quantitative traits shown, full results in Table S8.

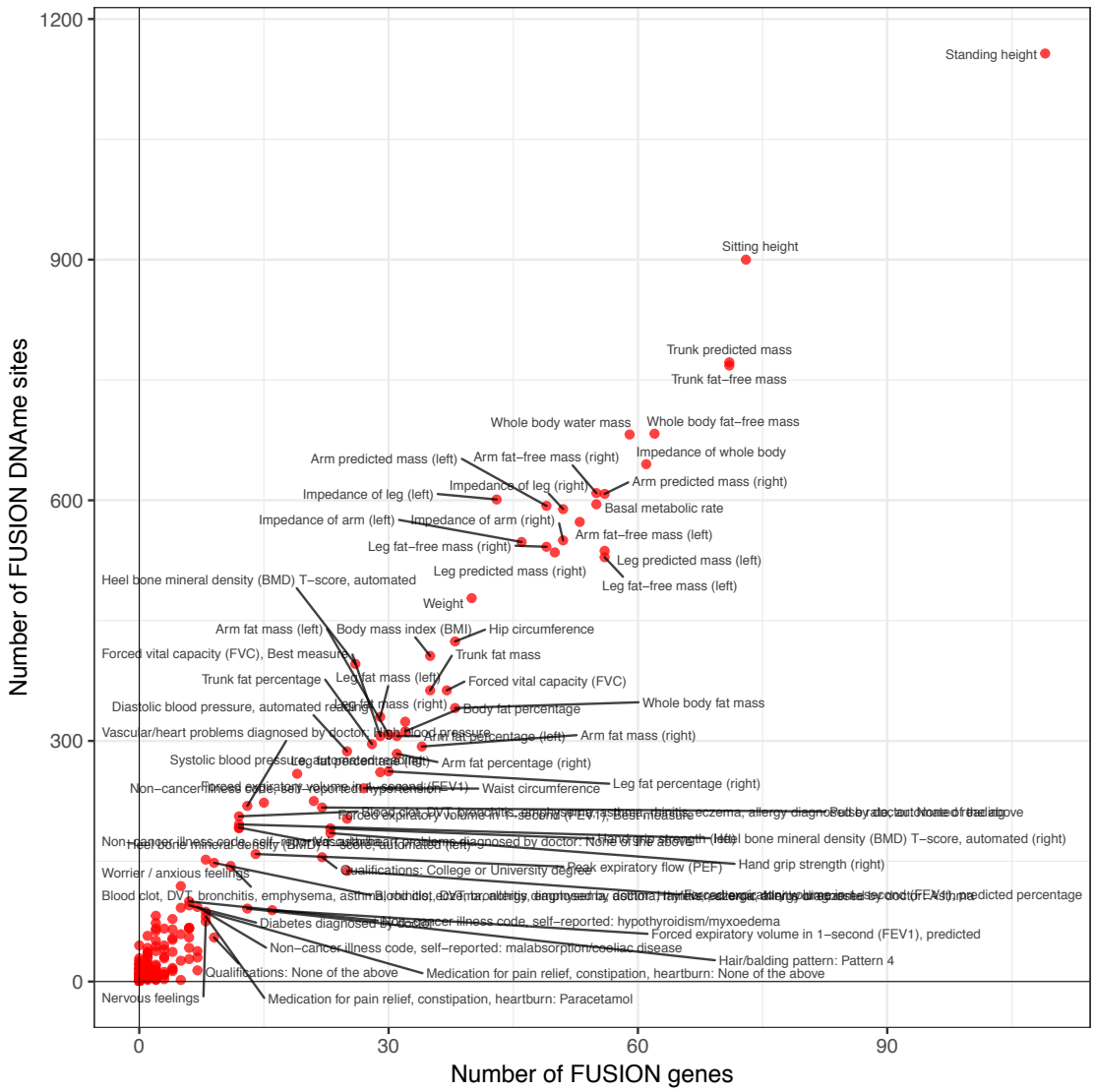

Fig. S25. Comparison of the number of FUSION gene expression and FUSION DNAme MR associations per disease/quantitative trait. Scatter plot of the number of genes (x-axis) and DNAme site (y-axis) MR associations (FDR$\leq 1\%$, $p_{\text{HEIDI}} > 0.05$, top QTL SNV has $p_{\text{GWAS}} \leq 5 * 10^{-8}$) for a disease/quantitative trait.

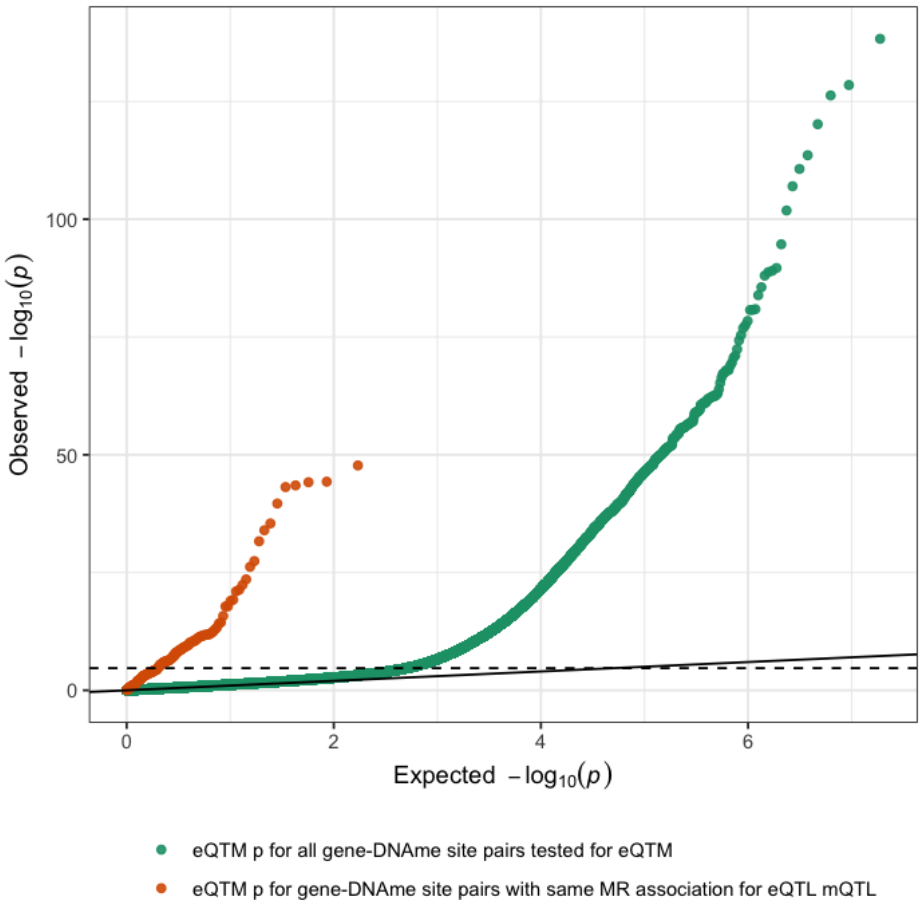

Fig. S26. Comparison of gene-DNAme site pairs from MR associations. Comparison of eQTM p-values of all gene-DNAme site pairs tested for eQTM (green) to 171 gene-DNAme site pairs identified through MR associations for the same disease/quantitative trait (orange). The solid black line is the identity line, and the dotted line corresponds to an eQTM FDR of 1%. 85 gene-DNAme site pairs without an eQTM are the orange points below the dashed line.

(A) Top eQTL SNV per tissue/study used as instrument.

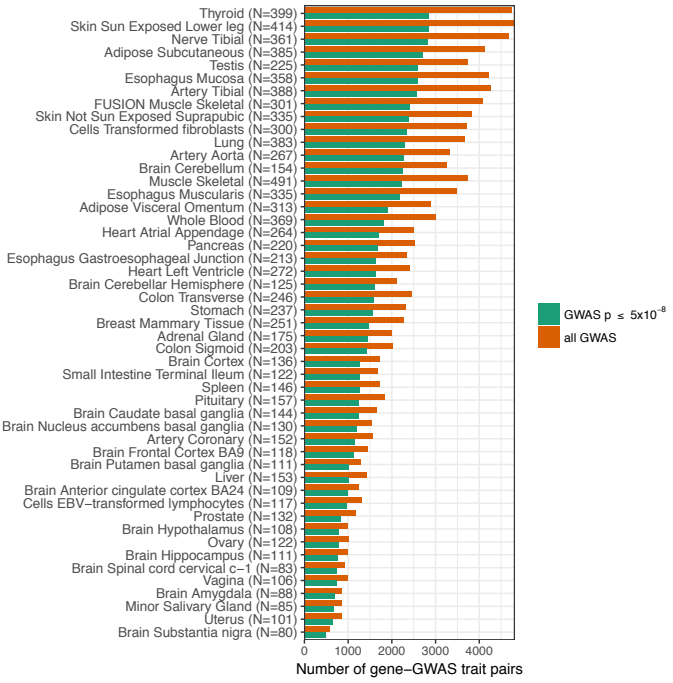

(B) Top FUSION eQTL SNV used as instrument.

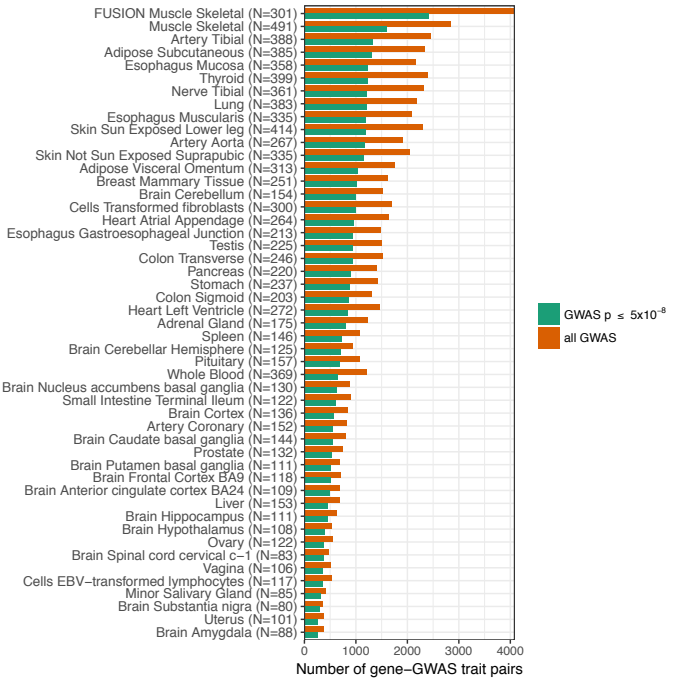

Fig. S27. Number of gene-disease/quantitative trait MR associations for FUSION skeletal muscle and GTEx tissues. Bar plots of number of genes with MR associations (FDR$\leq 1\%$, $p_{\text{HEIDI}} > 0.05$) for FUSION skeletal muscle and GTEx tissues, with (green) and without (orange) requiring top eQTL SNV to have a disease/quantitative trait $p_{\text{GWAS}} \leq 5 * 10^{-8}$. Number of samples used for eQTL mapping are given after each tissue name. (A) Top eQTL SNV per tissue/study used as instrument. (B) Top FUSION eQTL SNV used as instrument for FUSION skeletal muscle and GTEx tissues.

(A) GTEx skeletal muscle

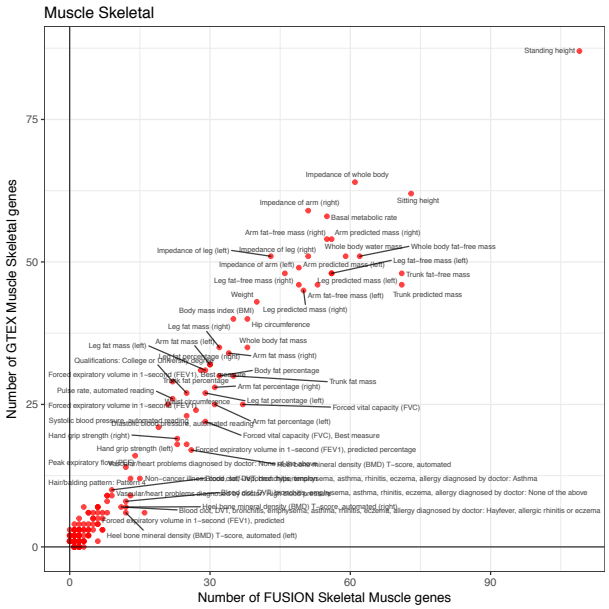

(B) GTEx skin (sun exposed lower leg)

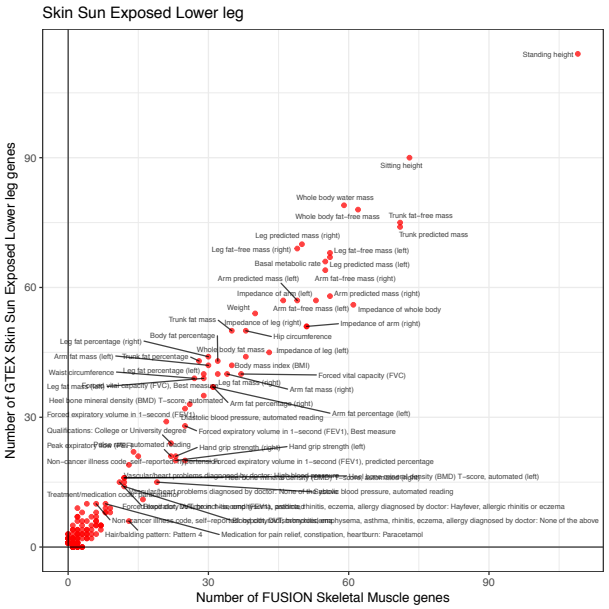

(C) GTEx thyroid

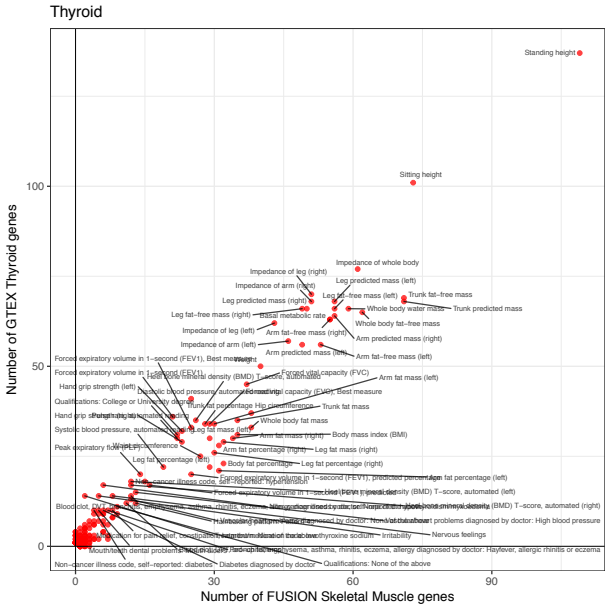

(D) GTEx brain substantia nigra

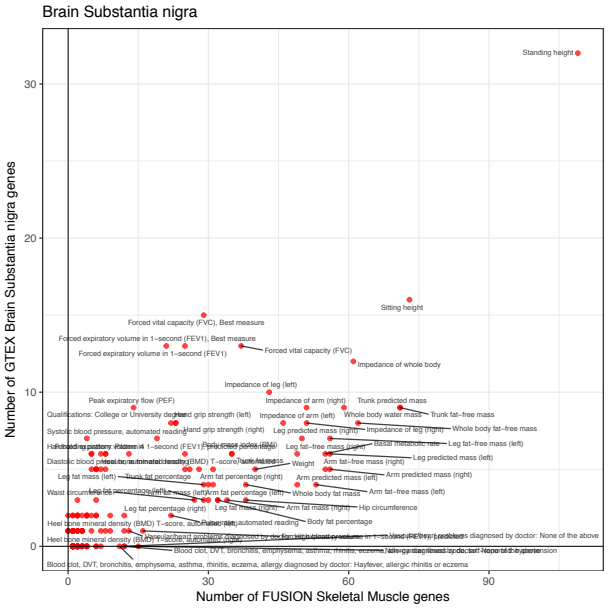

Fig. S28. Comparison of the number gene-disease/quantitative trait MR associations for FUSION skeletal muscle and selected GTEx tissues. Scatter plots of the number of FUSION skeletal muscle genes (x-axis) and number of GTEx tissue genes (y-axis) MR associations (FDR$\leq 1\%$, $p_{\text{HEIDI}} > 0.05$, top eQTL SNV has $p_{\text{GWAS}} \leq 5 * 10^{-8}$) for a disease/quantitative trait (point). Plots of FUSION skeletal muscle vs the following tissues: (A) GTEx skeletal muscle. (B) GTEx skin (sun exposed lower leg). (C) GTEx thyroid. (D) GTEx brain substantia nigra (least correlated with FUSION results).

(A) MR associations with top eQTL SNV $p_{\text{GWAS}} \leq 5 * 10^{-8}$

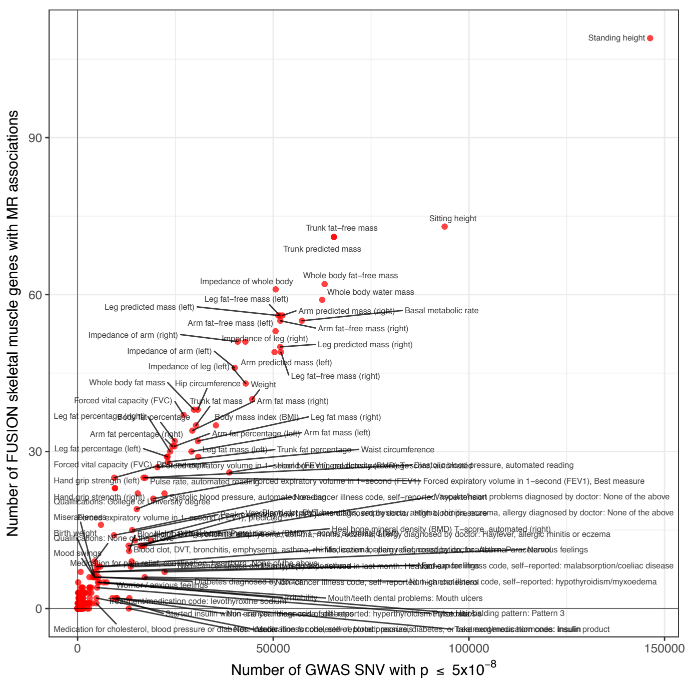

(B) MR associations without top eQTL SNV $p_{\text{GWAS}} \leq 5 * 10^{-8}$

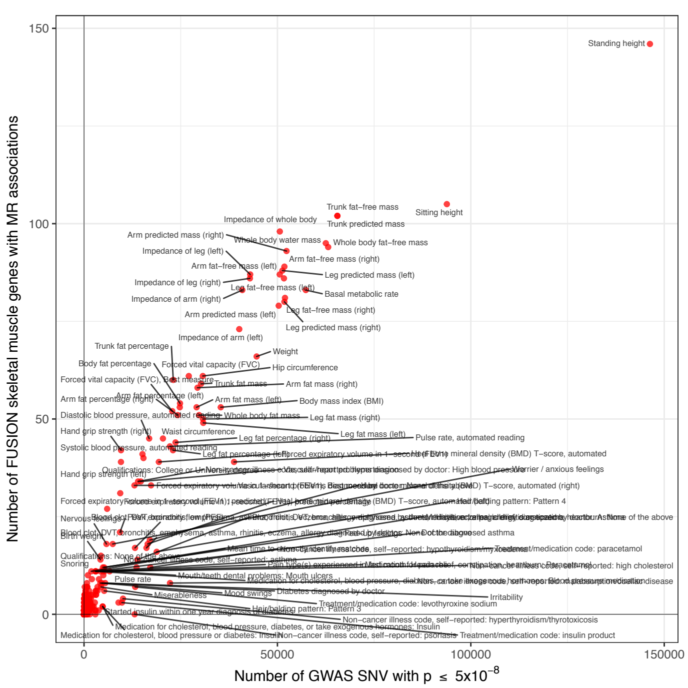

Fig. S29. Comparison of the number of MR associations per disease/quantitative trait and the number of disease/quantitative trait SNVs where $p_{\text{GWAS}} \leq 5 * 10^{-8}$. Comparison of the number of MR associations per disease/quantitative trait (y-axis) to the number of disease/quantitative trait SNVs with $p_{\text{GWAS}} \leq 5 * 10^{-8}$ (x-axis). (A) Top eQTL SNV required to have a disease/quantitative trait $p_{\text{GWAS}} \leq 5 * 10^{-8}$. (B) Top eQTL SNV not required to have a disease/quantitative trait $p_{\text{GWAS}} \leq 5 * 10^{-8}$.

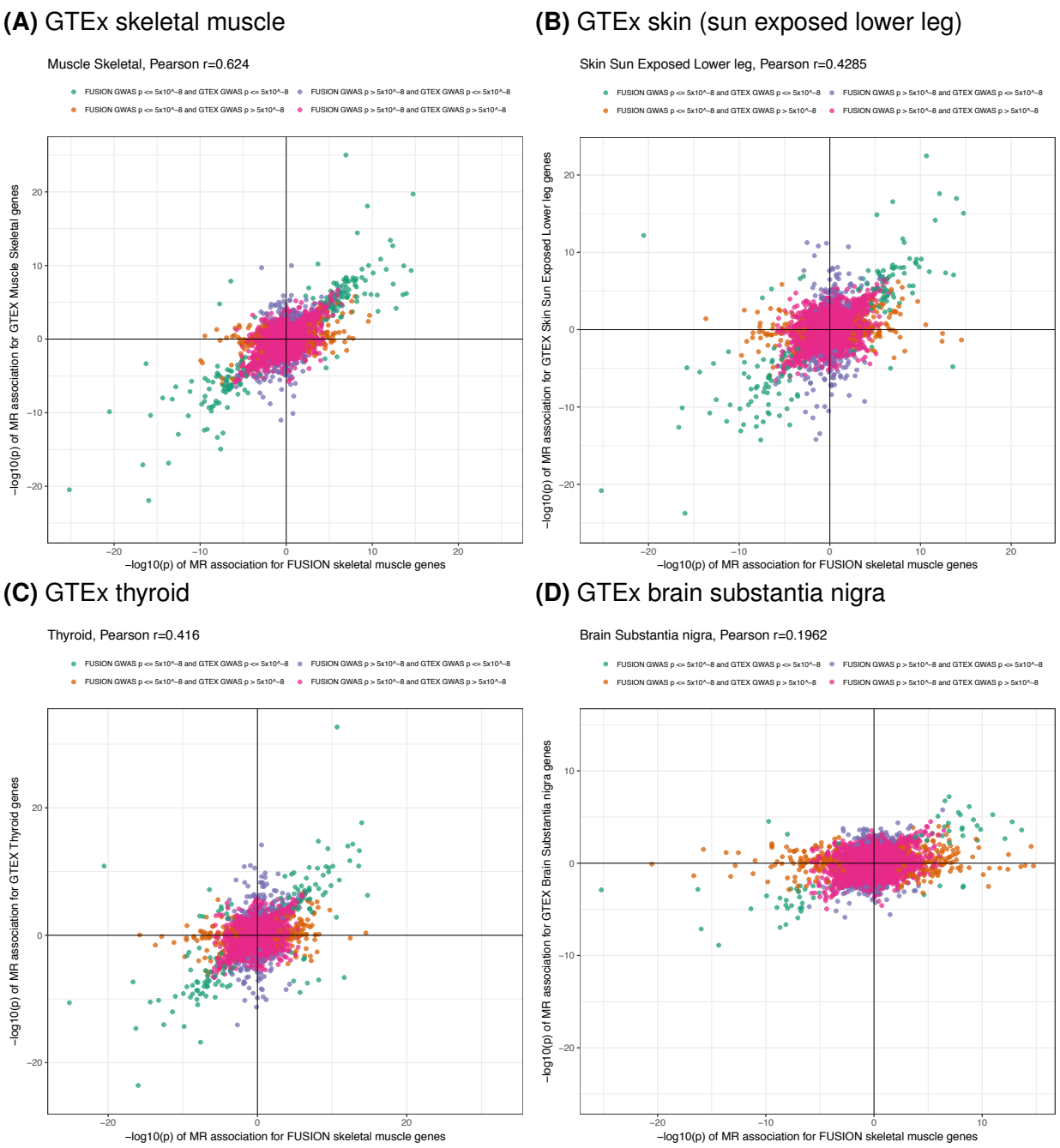

Fig. S30. Comparison of the strength and direction of gene expression-trunk predicted mass GWAS MR associations for FUSION skeletal muscle and selected GTEx tissues. Scatter plots of the signed (by MR effect) $-log_{10}$(gene expression-trunk predicted mass GWAS MR p-value) for selected GTEx tissues (y-axis) and FUSION skeletal muscle (x-axis). Each point represents a gene, and for each gene the top eQTL SNV per tissue/study was used as an instrument. Pearson's r is reported in subtitle. Plots of the following tissues vs FUSION skeletal muscle: (A) GTEx skeletal muscle. (B) GTEx skin (sun exposed lower leg). (C) GTEx thyroid. (D) GTEx brain substantia nigra (least correlated with FUSION results).

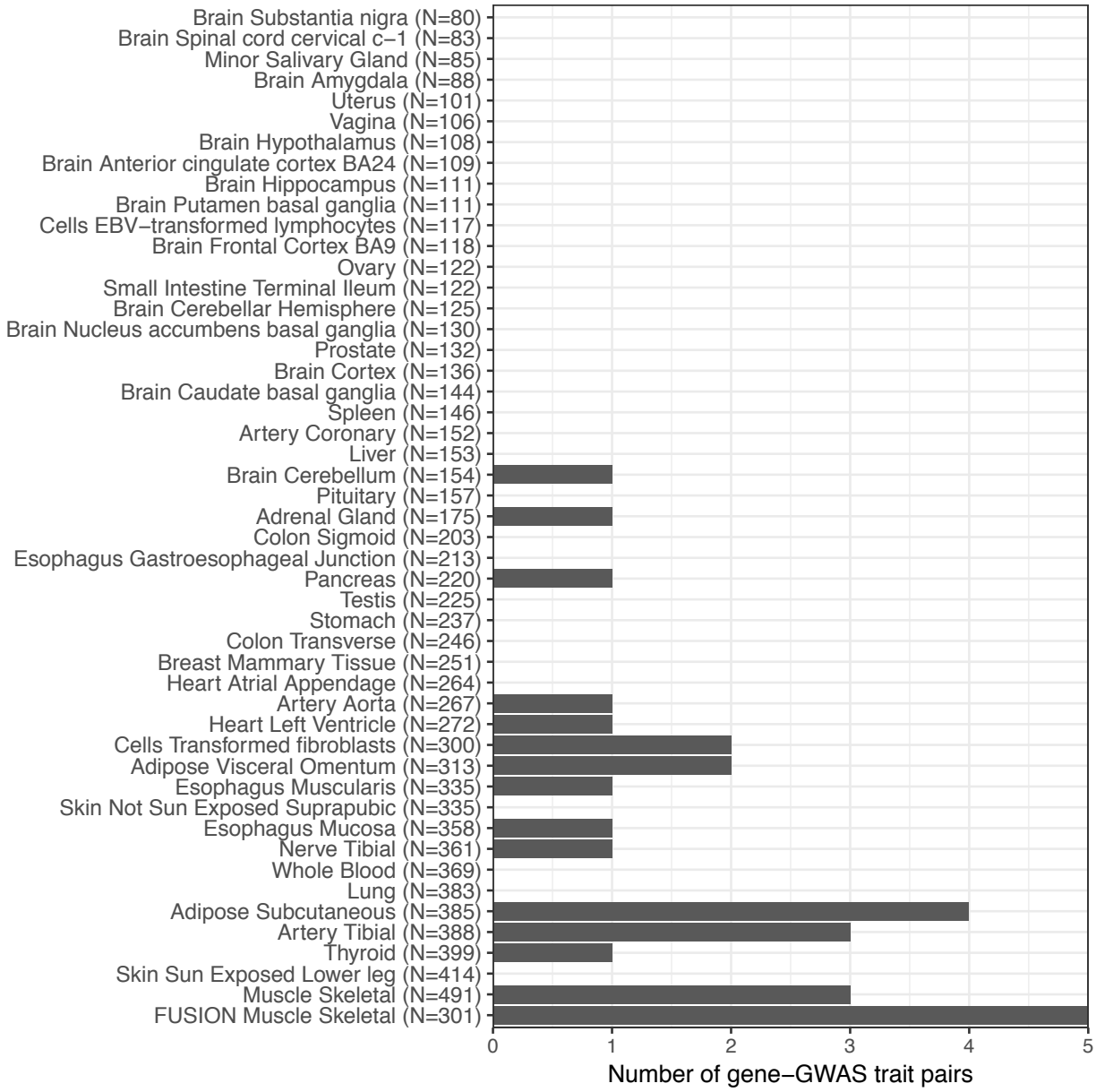

Fig. S31. Comparison of gene expression MR associations for T2D across for FUSION and GTEx. Bar plot depicting the number of gene expression MR associations (FDR$\leq 1\%$, $p_{\text{HEIDI}} > 0.05$, top eQTL SNV has $p_{\text{GWAS}} \leq 5 * 10^{-8}$) for T2D (x-axis) across GTEx tissues and FUSION skeletal muscle (y-axis). Number of samples used for eQTL mapping are given after each tissue name.

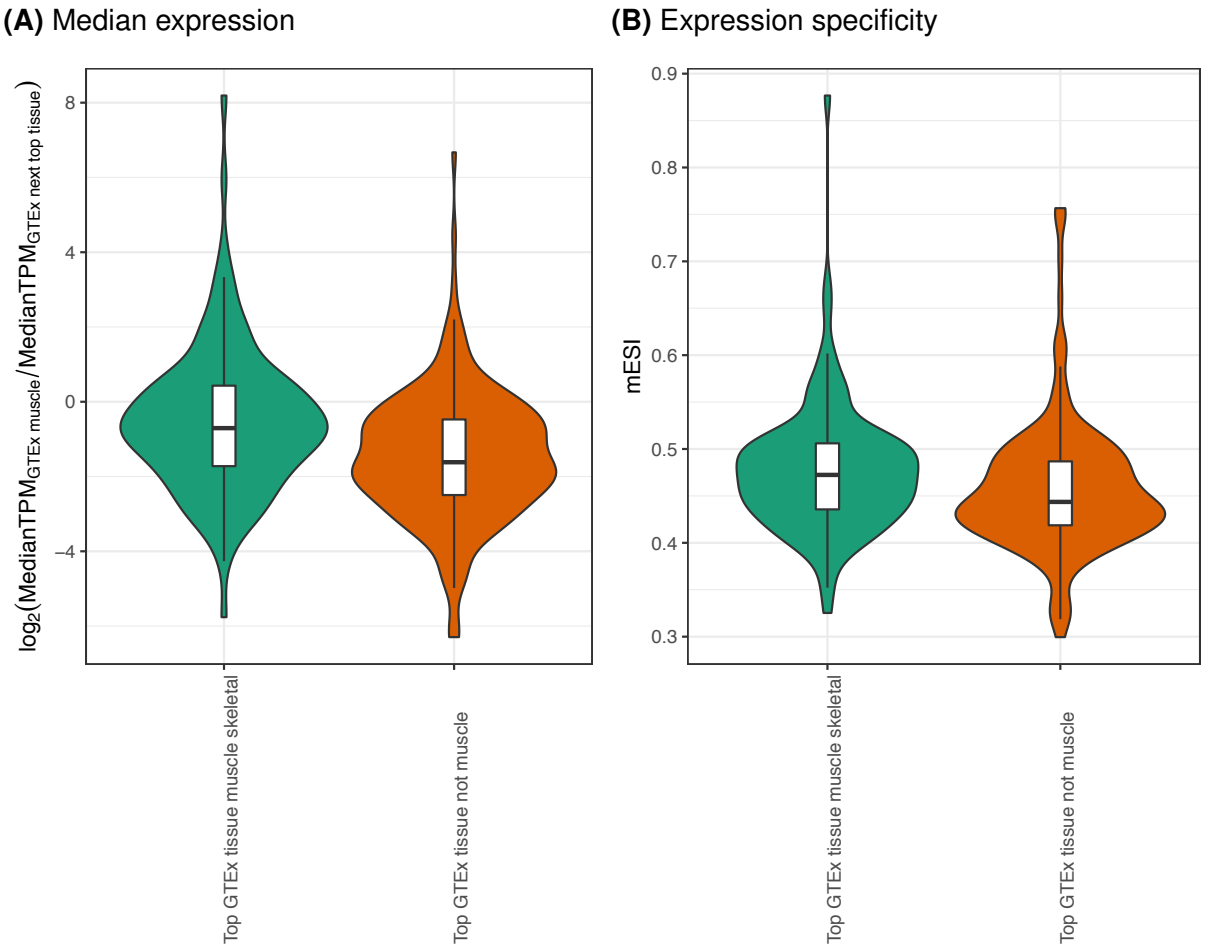

Fig. S32. Expression characteristics of genes with disease/quantitative trait MR association in FUSION that occur in GTEx skeletal muscle. Box plot of expression characteristics of genes where GTEx skeletal muscle is the strongest MR association across all GTEx tissues (green) and is not (orange). (A) The fold difference in expression of GTEx skeletal muscle and the GTEx tissue with the strongest MR association that is not GTEx skeletal muscle. (B) The skeletal muscle expression specificity index (mESI).

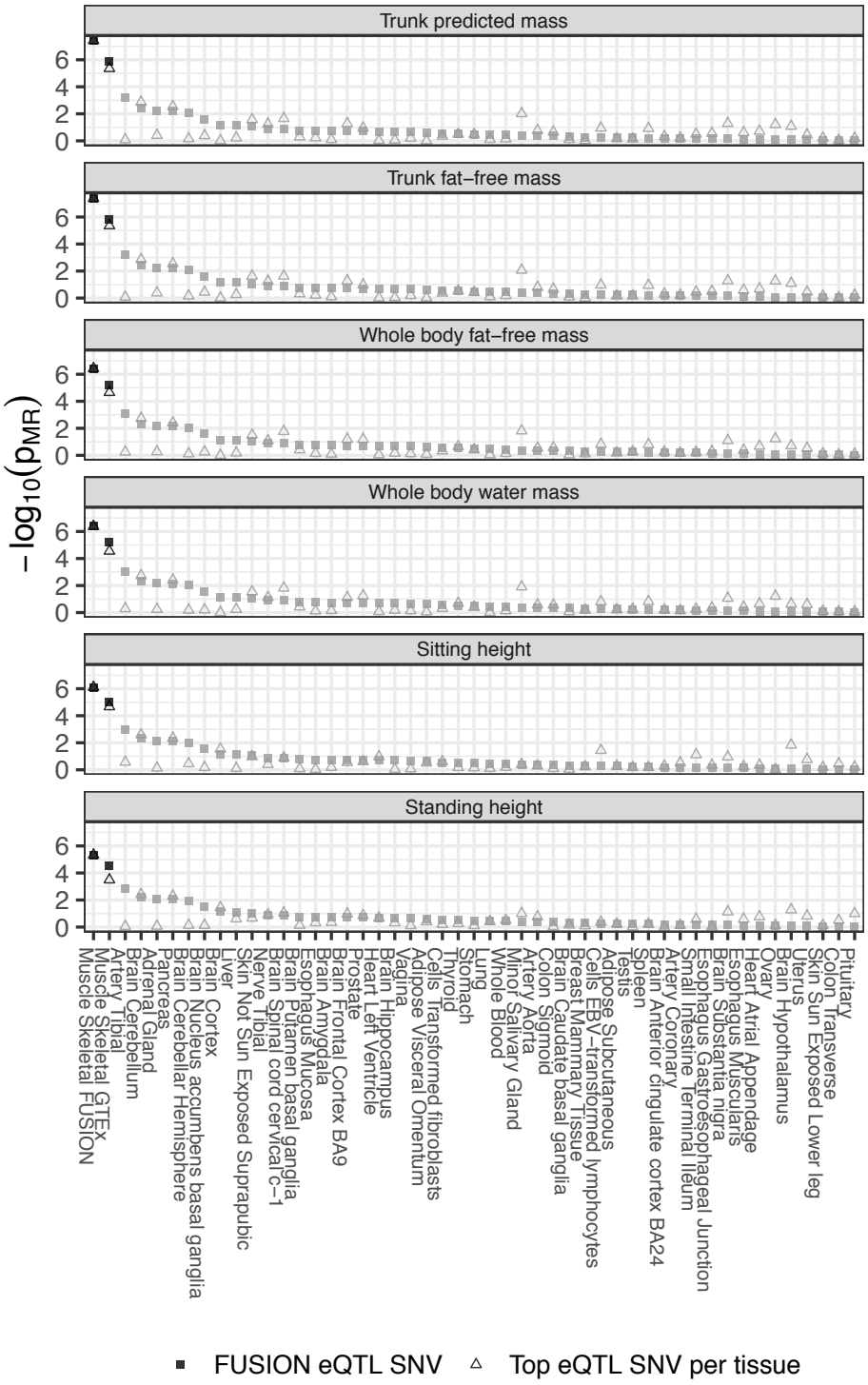

Fig. S33. *RXRA* MR associations for selected traits. Strength of MR association (y-axis) for FUSION skeletal muscle and GTEx tissues (x-axis) the top *RXRA*-eQTL SNV from FUSION (rs6583658; denoted with square) or the top GTEx tissue-specific *RXRA*-eQTL SNV (denoted with triangle) as the instrument. Panels split by GWAS traits.

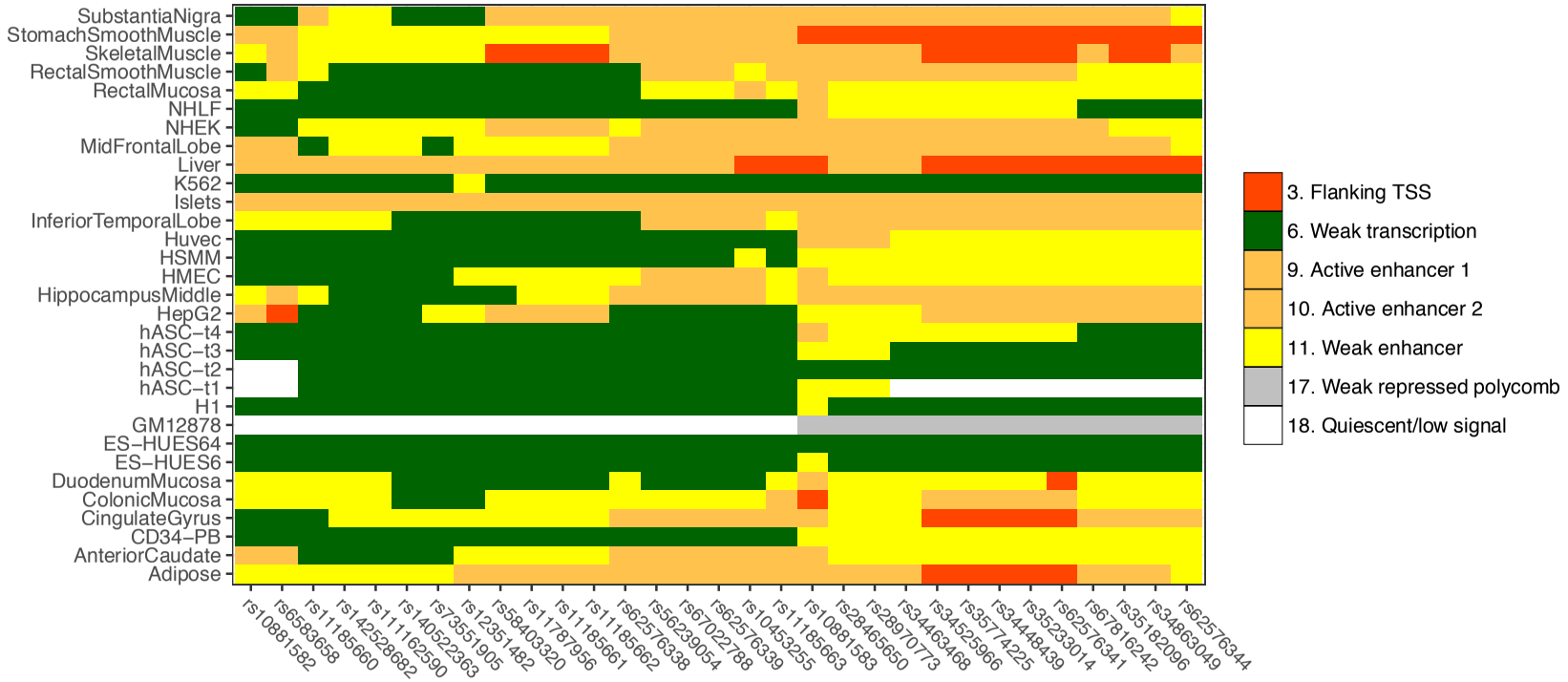

Fig. S34. rs6583658 chromatin states. Tissue/cell type chromatin states at rs6583658 and variants in LD with rs6583658 ($r^2 > 0.8$).

Supplementary Tables

Table S1. Characterization of participants in the FUSION tissue biopsy study.

	DNAme samples	RNA-seq samples	Common RNA-seq & DNAme samples	Union RNA-seq & DNAme samples
N	282	301	265	318
Sex = M (%)	159 (56.4%)	174 (57.8%)	152 (57.4%)	181 (56.9%)
Age (mean ± sd)	59.98 ± 7.92	59.91 ± 7.66	59.87 ± 7.72	60.01 ± 7.84
BMI (kg/m2; mean ± sd)	27.61 ± 4.27	27.45 ± 4.13	27.45 ± 4.14	27.59 ± 4.25
Fasting Serum Insulin (mU/l; mean ± sd)	8.83 ± 5.43	8.59 ± 5.20	8.66 ± 5.31	8.74 ± 5.32
Fasting Plasma Glucose (mmol/l; mean ± sd)	6.26 ± 0.78	6.27 ± 0.78	6.27 ± 0.79	6.26 ± 0.78
Ever Smoker = Y (%)	40 (14.2%)	43 (14.3%)	39 (14.7%)	44 (13.8%)
Oral Glucose Tolerance Test Status (%)				
Normal Glucose Tolerance (NGT)	98 (34.8%)	108 (35.9%)	90 (34.0%)	116 (36.5%)
Impaired Fasting Glucose (IFG)	39 (13.8%)	43 (14.3%)	38 (14.3%)	44 (13.8%)
Impaired Glucose Tolerance (IGT)	73 (25.9%)	73 (24.3%)	71 (26.8%)	75 (23.6)
Type 2 Diabetes (T2D)	72 (25.5%)	77 (25.6%)	66 (24.9%)	83 (26.1%)

Table S2A. Physiological trait associations with tissue type proportions. Linear regression analysis of inverse normalized trait with indicator variables for estimated tissue composition proportion adjusted for base covariates (***Methods***) and fiber type. The reference tissue is skeletal muscle.

Physiological trait	Tissue type coefficient			Tissue type p-value			F test for tissue
	Adipose	Lympho cytes	Whole blood	Adipose	Lymphoc ytes	Whole blood	
Waist	3.53	-96.1	34.81	0.13	0.33	0.074	0.070
BMI	4.41	-118.0	48.1	0.081	0.26	0.022	0.014
Fasting insulin	-0.46	190.0	47.7	0.86	0.075	0.024	0.0069
Weight	3.55	-23.5	35.3	0.094	0.79	0.045	0.028
WHR	1.73	-57.4	29.1	0.38	0.49	0.076	0.18
Fasting glucose	-0.79	-74.7	59.6	0.74	0.45	0.0026	0.025
T2D	-1.94	-87.8	99.7	0.78	0.77	0.11	0.42
Height	-0.36	69.5	-4.90	0.84	0.34	0.74	0.81

Table S2B. Physiological trait associations with fiber type proportions. Linear regression analysis of the inverse normalized trait with indicator variables for estimated fiber type proportion adjusted for base covariates (***Methods***) and tissue type. The reference fiber type is type 1.

Physiological trait	Fiber type coefficient		Fiber type p-value		F test for fiber type
	Type 2A	Type 2X	Type 2A	Type 2X	
Waist	-0.33	2.06	0.49	2.0×10^{-6}	5.1×10^{-7}
BMI	-0.72	2.00	0.17	1.9×10^{-5}	1.1×10^{-6}
Fasting insulin	-0.47	2.14	0.38	6.5×10^{-6}	1.2×10^{-6}
Weight	-0.57	1.40	0.20	4.1×10^{-4}	5.1×10^{-5}
WHR	0.0094	1.45	0.98	8.4×10^{-5}	1.4×10^{-4}
Fasting glucose	-0.73	0.32	0.16	0.48	0.16
T2D	-1.65	1.80	0.31	0.23	0.13
Height	-0.12	-0.42	0.74	0.20	0.44

Table S3. Sources of summary statistics for genetic effects on disease/quantitative traits.

Trait	Reference
T2D	(54)
Fasting glucose	(55)
Fasting insulin	(55)
HOMA	(55)
HOMA-B	(55)
Proinsulin	(56)
Proinsulin adjusted for BMI	(56)
BMI	(57)
Waist	(58)
Waist adjusted for BMI	(58)
Weight (men)	(59)
Weight (women)	(59)
UK Biobank traits Manifest 20170915 (downloaded Feb. 26, 2018)	(48) https://docs.google.com/spreadsheets/d/1b3oGI2lUt57BcuHttWaZotQcl0-mBRPyZihz87Ms_No

Table S4. Dropped UK Biobank traits. UK Biobank traits that were not considered in analysis.

Trait code	Trait description
2473	Other serious medical condition/disability diagnosed by doctor
2492	Taking other prescription medications
2844	Had other major operations
4825	Noisy workplace
20161	Pack years of smoking PREVIEW ONLY
20162	Pack years adult smoking as proportion of life span exposed to smoking PREVIEW ONLY
20002_99999	Non-cancer illness code, self-reported: unclassifiable
20107_100	Illnesses of father: None of the above (group 1)
20107_101	Illnesses of father: None of the above (group 2)
20110_100	Illnesses of mother: None of the above (group 1)
20110_101	Illnesses of mother: None of the above (group 2)
20111_100	Illnesses of siblings: None of the above (group 1)
20111_101	Illnesses of siblings: None of the above (group 2)
20118_11	Home area population density - urban or rural: Scotland - Large Urban Area
20118_12	Home area population density - urban or rural: Scotland - Other Urban Area
20118_13	Home area population density - urban or rural: Scotland - Accessible Small Town
20118_16	Home area population density - urban or rural: Scotland - Accessible Rural
20118_17	Home area population density - urban or rural: Scotland - Remote Rural
20118_3	Home area population density - urban or rural: England/Wales - Village - sparse
20118_6	Home area population density - urban or rural: England/Wales - Town and Fringe - less sparse
20118_7	Home area population density - urban or rural: England/Wales - Village - less sparse
20118_8	Home area population density - urban or rural: England/Wales - Hamlet and Isolated Dwelling - less sparse
20118_9	Home area population density - urban or rural: Postcode not linkable
2664_1	Reason for reducing amount of alcohol drunk: Illness or ill health
2664_2	Reason for reducing amount of alcohol drunk: Doctor's advice
2664_3	Reason for reducing amount of alcohol drunk: Health precaution
2664_4	Reason for reducing amount of alcohol drunk: Financial reasons
3859_1	Reason former drinker stopped drinking alcohol: Illness or ill health
3859_3	Reason former drinker stopped drinking alcohol: Health precaution
6155_100	Vitamin and mineral supplements: None of the above
6157_1	Why stopped smoking: Illness or ill health
6157_100	Why stopped smoking: None of the above
6157_2	Why stopped smoking: Doctor's advice
6157_3	Why stopped smoking: Health precaution

6157_4	Why stopped smoking: Financial reasons
6158_1	Why reduced smoking: Illness or ill health
6158_100	Why reduced smoking: None of the above
6158_2	Why reduced smoking: Doctor's advice
6158_3	Why reduced smoking: Health precaution
6158_4	Why reduced smoking: Financial reasons
6179_100	Mineral and other dietary supplements: None of the above
A63	Diagnoses - main ICD10: A63 Other predominantly sexually transmitted diseases, not elsewhere classified
R68	Diagnoses - main ICD10: R68 Other general symptoms and signs
Z51	Diagnoses - main ICD10: Z51 Other medical care
Z53	Diagnoses - main ICD10: Z53 Persons encountering health services for specific procedures, not carried out
Z71	Diagnoses - main ICD10: Z71 Persons encountering health services for other counselling and medical advice, not elsewhere classified
Z76	Diagnoses - main ICD10: Z76 Persons encountering health services in other circumstances
6142_100	Current employment status: None of the above

Table S5. Genotype QC summary. Genotype QC summary of all FUSION biopsy samples.

Samples Removed	Description
2	One sample from each of 2 first degree relative pairs (drop NGT and keep IGT in both cases). Identified in Scott et al. (4).
1	Non-Finnish participant.
328 / 331	*Total samples passed / total samples submitted*

Table S6. RNA-seq QC summary. RNA-seq QC summary on skeletal muscle samples.

Samples Removed	Description
1	Contaminated with a different sample based on genotype comparison. Identified in Scott et al. (4).
4	Extreme 3' bias in gene body coverage. One sample identified in Scott et al. (4).
7	Outlier in transcriptional diversity.
2	Drop one of 2 pairs of first degree relatives (genotype QC; Table S5).
1	Drop non-Finnish participant (genotype QC; Table S5).
7	Select one sample from 6 intentional replicates and one unintentional replicate.
301 / 323	*Total samples passed / total samples submitted*

Table S7. DNAme QC summary. DNAme QC summary on skeletal muscle samples.

Samples Removed	Description
5	Failed low quality probe filter.
1	Outlier in median raw methylated and un-methylated signals across probes.
3	Outlier in control probes.
4	Contaminated with a different sample based on genotype comparison.
1	Outlier in DNAme distribution.
3	Clustered outside expected tissue in PCA.
1	Failed residual PCA filter.
2	Drop one of 2 pairs of first degree relatives (genotype QC; Table S5).
1	Drop non-Finnish participant (genotype QC; Table S5).
282 / 303	*Total samples passed / total samples submitted*

Captions for Supplementary Datasets

Dataset S1A. Top 50 genes associated with skeletal muscle fiber type proportions. (separate file). P-values adjusted using the Benjamini-Hochberg procedure. Type1 fiber used as reference.

Dataset S1B. Top 50 DNAme sites associated with skeletal muscle fiber type proportions. (separate file). P-values adjusted using the Benjamini-Hochberg procedure. Type1 fiber used as reference.

Dataset S2. Predicted causal direction for gene-DNAme site pairs. (separate file).

Dataset S3. Number of FUSION gene expression MR associations per disease/quantitative trait. (separate file). Number of gene-trait pairs (FDR≤1%, p_{HEIDI}>0.05) for each disease/quantitative trait with and without requiring the top eQTL SNV to have a disease/quantitative trait $p_{GWAS} \leq 5x10^{-8}$.

Dataset S4. Number of FUSION DNAme MR associations per disease/quantitative trait. (separate file). Number of DNAme site-trait pairs (FDR≤1%, p_{HEIDI}>0.05) for each disease/quantitative trait with and without requiring the top mQTL SNV to have a disease/quantitative trait $p_{GWAS} \leq 5x10^{-8}$.

Dataset S5. FUSION and GTEx muscle MR associations. (separate file). Overlapping FUSION muscle and GTEx muscle MR associations where the GTEx muscle MR association was the smallest among all other GTEx tissues.

References

1. Gutierrez-Arcelus M, et al. (2013) Passive and active DNA methylation and the interplay with genetic variation in gene regulation. *elife* 2:e00523.
2. Ng B, et al. (2017) An xQTL map integrates the genetic architecture of the human brain's transcriptome and epigenome. *Nat Neurosci* 20(10):1418–1426.
3. Hemani G, Tilling K, Davey Smith G (2017) Orienting the causal relationship between imprecisely measured traits using GWAS summary data. *PLoS Genet* 13(11):e1007081.
4. Scott LJ, et al. (2016) The genetic regulatory signature of type 2 diabetes in human skeletal muscle. *Nat Commun* 7:11764.
5. Li H, Durbin R (2009) Fast and accurate short read alignment with Burrows-Wheeler transform. *Bioinformatics* 25(14):1754–1760.
6. Manichaikul A, et al. (2010) Robust relationship inference in genome-wide association studies. *Bioinformatics* 26(22):2867–2873.
7. Novembre J, et al. (2008) Genes mirror geography within Europe. *Nature* 456(7218):98–101.
8. Taliun D, et al. (2017) LASER server: ancestry tracing with genotypes or sequence reads. *Bioinformatics* 33(13):2056–2058.
9. Price AL, et al. (2006) Principal components analysis corrects for stratification in genome-wide association studies. *Nat Genet* 38(8):904–909.
10. Price AL, et al. (2008) Long-range LD can confound genome scans in admixed populations. *Am J Hum Genet* 83(1):132–135.
11. Weale ME (2010) Quality control for genome-wide association studies. *Methods Mol Biol* 628:341–372.
12. Das S, et al. (2016) Next-generation genotype imputation service and methods. *Nat Genet* 48(10):1284–1287.
13. Loh P-R, et al. (2016) Reference-based phasing using the Haplotype Reference Consortium panel. *Nat Genet* 48(11):1443–1448.
14. McCarthy S, et al. (2016) A reference panel of 64,976 haplotypes for genotype imputation. *Nat Genet* 48(10):1279–1283.
15. Gallego Romero I, Pai AA, Tung J, Gilad Y (2014) RNA-seq: impact of RNA degradation on transcript quantification. *BMC Biol* 12:42.
16. Wang L, et al. (2016) Measure transcript integrity using RNA-seq data. *BMC Bioinformatics* 17:58.
17. Wang L, Wang S, Li W (2012) RSeQC: quality control of RNA-seq experiments. *Bioinformatics* 28(16):2184–2185.

18. Harrow J, et al. (2012) GENCODE: the reference human genome annotation for The ENCODE Project. *Genome Res* 22(9):1760–1774.
19. Anders S, Pyl PT, Huber W (2015) HTSeq — a Python framework to work with high-throughput sequencing data. *Bioinformatics* 31(2):166–169.
20. Wagner GP, Kin K, Lynch VJ (2012) Measurement of mRNA abundance using RNA-seq data: RPKM measure is inconsistent among samples. *Theory Biosci* 131(4):281–285.
21. Li B, Ruotti V, Stewart RM, Thomson JA, Dewey CN (2010) RNA-Seq gene expression estimation with read mapping uncertainty. *Bioinformatics* 26(4):493–500.
22. Hartley SW, Mullikin JC (2015) QoRTs: a comprehensive toolset for quality control and data processing of RNA-Seq experiments. *BMC Bioinformatics* 16:224.
23. Jun G, et al. (2012) Detecting and estimating contamination of human DNA samples in sequencing and array-based genotype data. *Am J Hum Genet* 91(5):839–848.
24. Chen Y, et al. (2013) Discovery of cross-reactive probes and polymorphic CpGs in the Illumina Infinium HumanMethylation450 microarray. *Epigenetics* 8(2):203–209.
25. Price ME, et al. (2013) Additional annotation enhances potential for biologically-relevant analysis of the Illumina Infinium HumanMethylation450 BeadChip array. *Epigenetics Chromatin* 6(1):4.
26. McCartney DL, et al. (2016) Identification of polymorphic and off-target probe binding sites on the Illumina Infinium MethylationEPIC BeadChip. *Genom Data* 9:22–24.
27. Zhang X, Mu W, Zhang W (2012) On the analysis of the Illumina 450k array data: probes ambiguously mapped to the human genome. *Front Genet* 3:73.
28. Aryee MJ, et al. (2014) Minfi: a flexible and comprehensive Bioconductor package for the analysis of Infinium DNA methylation microarrays. *Bioinformatics* 30(10):1363–1369.
29. Dedeurwaerder S, et al. (2014) A comprehensive overview of Infinium HumanMethylation450 data processing. *Brief Bioinformatics* 15(6):929–941.
30. Fortin J-P, Fertig E, Hansen K (2014) shinyMethyl: interactive quality control of Illumina 450k DNA methylation arrays in R. [version 2; peer review: 2 approved]. *F1000Res* 3:175.
31. Love MI, Huber W, Anders S (2014) Moderated estimation of fold change and dispersion for RNA-seq data with DESeq2. *Genome Biol* 15(12):550.

32. Schiaffino S, Reggiani C (2011) Fiber types in mammalian skeletal muscles. *Physiol Rev* 91(4):1447–1531.

33. Benjamini Y, Hochberg Y (1995) Controlling the false discovery rate: A practical and powerful approach to multiple testing. *Journal of the Royal Statistical Society Series B (Methodological)* 57(1):289–300.

34. Lee C, Patil S, Sartor MA (2016) RNA-Enrich: a cut-off free functional enrichment testing method for RNA-seq with improved detection power. *Bioinformatics* 32(7):1100–1102.

35. Lippert C, Casale FP, Rakitsch B, Stegle O (2014) LIMIX: genetic analysis of multiple traits. *BioRxiv*.

36. Popadin K, Gutierrez-Arcelus M, Dermitzakis ET, Antonarakis SE (2013) Genetic and epigenetic regulation of human lincRNA gene expression. *Am J Hum Genet* 93(6):1015–1026.

37. Wagner JR, et al. (2014) The relationship between DNA methylation, genetic and expression inter-individual variation in untransformed human fibroblasts. *Genome Biol* 15(2):R37.

38. Chen L, et al. (2016) Genetic drivers of epigenetic and transcriptional variation in human immune cells. *Cell* 167(5):1398–1414.e24.

39. Cole SR, et al. (2010) Illustrating bias due to conditioning on a collider. *Int J Epidemiol* 39(2):417–420.

40. Delaneau O, et al. (2017) A complete tool set for molecular QTL discovery and analysis. *Nat Commun* 8:15452.

41. Stegle O, Parts L, Durbin R, Winn J (2010) A Bayesian framework to account for complex non-genetic factors in gene expression levels greatly increases power in eQTL studies. *PLoS Comput Biol* 6(5):e1000770.

42. Storey JD, Tibshirani R (2003) Statistical significance for genomewide studies. *Proc Natl Acad Sci USA* 100(16):9440–9445.

43. Zhu Z, et al. (2016) Integration of summary data from GWAS and eQTL studies predicts complex trait gene targets. *Nat Genet* 48(5):481–487.

44. Wu Y, et al. (2018) Integrative analysis of omics summary data reveals putative mechanisms underlying complex traits. *Nat Commun* 9(1):918.

45. Fuchsberger C, et al. (2016) The genetic architecture of type 2 diabetes. *Nature* 536(7614):41–47.

46. Millstein J, Chen GK, Breton CV (2016) cit: hypothesis testing software for mediation analysis in genomic applications. *Bioinformatics* 32(15):2364–2365.

47. Millstein J, Zhang B, Zhu J, Schadt EE (2009) Disentangling molecular relationships with a causal inference test. *BMC Genet* 10:23.

48. Churchhouse C, Neale B (2017) Rapid GWAS of thousands of phenotypes for 337,000 samples in the UK Biobank. *Neale lab*. Available at: http://www.nealelab.is/blog/2017/7/19/rapid-gwas-of-thousands-of-phenotypes-for-337000-samples-in-the-uk-biobank [Accessed July 30, 2018].
49. Howrigan D (2017) Details and considerations of the UK Biobank GWAS. *Neale lab*. Available at: http://www.nealelab.is/blog/2017/9/11/details-and-considerations-of-the-uk-biobank-gwas [Accessed July 27, 2018].
50. Smith Davey G, Ebrahim S (2003) “Mendelian randomization”: can genetic epidemiology contribute to understanding environmental determinants of disease? *Int J Epidemiol* 32(1):1–22.
51. Varshney A, et al. (2017) Genetic regulatory signatures underlying islet gene expression and type 2 diabetes. *Proc Natl Acad Sci USA* 114(9):2301–2306.
52. Buenrostro JD, Giresi PG, Zaba LC, Chang HY, Greenleaf WJ (2013) Transposition of native chromatin for fast and sensitive epigenomic profiling of open chromatin, DNA-binding proteins and nucleosome position. *Nat Methods* 10(12):1213–1218.
53. Allum F, et al. (2015) Characterization of functional methylomes by next-generation capture sequencing identifies novel disease-associated variants. *Nat Commun* 6:7211.
54. Scott RA, et al. (2017) An Expanded Genome-Wide Association Study of Type 2 Diabetes in Europeans. *Diabetes* 66(11):2888–2902.
55. Dupuis J, et al. (2010) New genetic loci implicated in fasting glucose homeostasis and their impact on type 2 diabetes risk. *Nat Genet* 42(2):105–116.
56. Strawbridge RJ, et al. (2011) Genome-wide association identifies nine common variants associated with fasting proinsulin levels and provides new insights into the pathophysiology of type 2 diabetes. *Diabetes* 60(10):2624–2634.
57. Speliotes EK, et al. (2010) Association analyses of 249,796 individuals reveal 18 new loci associated with body mass index. *Nat Genet* 42(11):937–948.
58. Shungin D, et al. (2015) New genetic loci link adipose and insulin biology to body fat distribution. *Nature* 518(7538):187–196.
59. Randall JC, et al. (2013) Sex-stratified genome-wide association studies including 270,000 individuals show sexual dimorphism in genetic loci for anthropometric traits. *PLoS Genet* 9(6):e1003500.